NASA TECHNICAL NOTE

NASA TN D-7358

NASA TN D-7358

HYPERSONIC AERODYNAMIC CHARACTERISTICS OF AN ALL-BODY RESEARCH AIRCRAFT CONFIGURATION

by Louis E. Clark

Langley Research Center
Hampton, Va. 23665

NATIONAL AERONAUTICS AND SPACE ADMINISTRATION • WASHINGTON, D. C. • DECEMBER 1973

1. Report No NASA TN D-7358	2. Government Accession No.	3. Recipient's Catalog No
4. Title and Subtitle HYPERSONIC AERODYNAMIC CHARACTERISTICS OF AN ALL-BODY RESEARCH AIRCRAFT CONFIGURATION		5. Report Date December 1973 6. Performing Organization Code
7. Author(s) Louis E. Clark		8. Performing Organization Report No L-8971 10. Work Unit No. 760-66-01-02
9. Performing Organization Name and Address NASA Langley Research Center Hampton, Va. 23665		11. Contract or Grant No 13. Type of Report and Period Covered Technical Note
12. Sponsoring Agency Name and Address National Aeronautics and Space Administration Washington, D.C. 20546		14. Sponsoring Agency Code
15. Supplementary Notes		

16. Abstract

An experimental investigation was conducted at Mach 6 to determine the hypersonic aerodynamic characteristics of an all-body, delta-planform, hypersonic research aircraft (HYFAC configuration). The aerodynamic characteristics were obtained at Reynolds numbers based on model length of 2.84×10^6 and 10.5×10^6 and over an angle-of-attack range from -4° to 20°.

The experimental results show that the HYFAC configuration is longitudinally stable and can be trimmed over the range of test conditions. The configuration had a small degree of directional stability over the angle-of-attack range and positive effective dihedral at angles of attack greater than 2°. Addition of canards caused a decrease in longitudinal stability and an increase in directional stability. Oil-flow studies revealed extensive areas of separated and vortex flow on the fuselage lee surface. A limited comparison of wind-tunnel data with several hypersonic approximations indicated that, except for the directional stability, the tangent-cone method gave adequate agreement at control settings between 5° and -5° and positive lift coefficient. A limited comparison indicated that the HYFAC configuration had greater longitudinal stability than an elliptical-cross-section configuration, but a lower maximum lift-drag ratio.

17. Key Words (Suggested by Author(s))	18. Distribution Statement		
Hypersonic stability All-body aircraft	Unclassified -- Unlimited		
19. Security Classif. (of this report) Unclassified	20. Security Classif. (of this page) Unclassified	21. No. of Pages 46	22. Price* Domestic, $3.00 Foreign, $5.50

*For sale by the National Technical Information Service, Springfield, Virginia 22151

HYPERSONIC AERODYNAMIC CHARACTERISTICS OF AN ALL-BODY RESEARCH AIRCRAFT CONFIGURATION

By Louis E. Clark
Langley Research Center

SUMMARY

An experimental investigation was conducted at Mach 6 to determine the hypersonic aerodynamic characteristics of an all-body, delta-planform, hypersonic research aircraft (HYFAC configuration). The aerodynamic characteristics were obtained at Reynolds numbers based on model length of 2.84×10^6 and 10.5×10^6 and over an angle-of-attack range from -4° to 20°.

The experimental results show that the HYFAC configuration is longitudinally stable and can be trimmed over the range of test conditions. The configuration had a small degree of directional stability over the angle-of-attack range and positive effective dihedral at angles of attack greater than 2°. Addition of canards caused a decrease in longitudinal stability and an increase in directional stability. Oil-flow studies revealed extensive areas of separated and vortex flow on the fuselage lee surface. A limited comparison of wind-tunnel data with several hypersonic approximations indicated that, except for the directional stability, the tangent-cone method gave adequate agreement at control settings between 5° and -5° and positive lift coefficient. A limited comparison indicated that the HYFAC configuration had greater longitudinal stability than an elliptical-cross-section configuration, but a lower maximum lift-drag ratio.

INTRODUCTION

The Hypersonic Research Facilities (HYFAC) study prepared by McDonnell Aircraft Company under a NASA contract defined several flight research vehicle concepts. (See refs. 1, 2, and 3.) One of these was a Mach 12 air-launched, rocket-accelerated, rocket-cruise, manned vehicle. This aircraft was an all-body design proposed as a test vehicle for liquid-hydrogen-fueled, scramjet-powered hypersonic flight and is referred to herein as the HYFAC configuration. The studies of all-body hypersonic cruise configurations are mainly theoretical, and experimental verification of their aerodynamic characteristics is needed.

The purpose of the present investigation was to determine the hypersonic aerodynamic characteristics at Mach 6 of the HYFAC all-body configuration, to determine problem regions of separated and vortex flow from oil-flow studies, and to make a limited comparison of the aerodynamic characteristics with several theoretical methods. The tests were conducted at Mach 6 at free-stream Reynolds numbers of 1.5×10^6 and 6.5×10^6; the angle of attack varied from -4° to 20° and the sideslip angle varied from 0° to 8°.

SYMBOLS AND COMPONENT DESIGNATIONS

The longitudinal forces and moments were referenced to the stability-axis system, and the lateral forces and moments were referenced to the body-axis system. The moment reference was located 30.79 cm (12.12 in.) aft of the model nose (64 percent of body length); the body length (48.11 cm (18.94 in.)) was used as the reference length in calculating the coefficients; and a reference area of 318.13 cm^2 (49.31 in^2) was used in calculating the coefficients. This area, determined by mechanical integration, includes the delta body, the horizontal control surfaces, and the area of the vertical tails except that which projects aft beyond the fuselage.

A_{max} maximum body cross-sectional area

b span (measured between body tips), 12.52 cm

C_D drag coefficient, $\frac{\text{Drag}}{q_\infty S}$

$C_{D,o}$ drag coefficient at zero lift

C_L lift coefficient, $\frac{\text{Lift}}{q_\infty S}$

C_{L_α} lift-curve slope at zero lift, $\frac{\partial C_L}{\partial \alpha}$, per deg

C_l rolling-moment coefficient, $\frac{\text{Rolling moment}}{q_\infty S b}$

C_{l_β} effective-dihedral parameter, $\frac{\partial C_l}{\partial \beta}$, per deg

C_m pitching-moment coefficient, $\frac{\text{Pitching moment}}{q_\infty S \bar{c}}$

C_{m_α} pitching-moment-curve slope, $\frac{\partial C_m}{\partial \alpha}$

C_n	yawing-moment coefficient, $\frac{\text{Yawing moment}}{q_\infty Sb}$
C_{n_β}	directional-stability parameter, $\frac{\partial C_n}{\partial \beta}$, per deg
C_Y	side-force coefficient, $\frac{\text{Side force}}{q_\infty S}$
C_{Y_β}	side-force parameter, $\frac{\partial C_Y}{\partial \beta}$, per deg
K	Newtonian correlation factor
L/D	lift-drag ratio
l	body length, 48.11 cm, used as reference length for pitching moment
M	Mach number
q_∞	free-stream dynamic pressure
$R_{\infty,l}$	Reynolds number based on body length
S	reference area, 318.13 cm^2
z_{cg}	vertical distance of center of gravity from model center line
α	angle of attack, deg
β	angle of sideslip, deg
δ_c	canard deflection angle, deg (negative when trailing edge is up)
δ_h	horizontal stabilizer angle, deg (negative when trailing edge is up)
$\delta_{h,L}$	left horizontal stabilizer angle, deg
$\delta_{h,R}$	right horizontal stabilizer angle, deg
Λ	body sweep angle, deg

Subscripts:

max	maximum
trim	trimmed condition
∞	free stream

Model component designations:

B	body
C_B	large canard
C_S	small canard
H	horizontal tail or stabilizer
V	vertical tail

APPARATUS AND TESTS

The tests were conducted in the Langley 20-inch Mach 6 tunnel. This is a blowdown-type wind tunnel with a two-dimensional nozzle and a test section 52.1 cm (20.5 in.) high and 50.8 cm (20 in.) wide. This facility is discussed in more detail in reference 4.

Tests were conducted at free-stream Reynolds numbers based on model length of 2.84×10^6 and 10.5×10^6. The angle of attack varied from -4° to 20° and the sideslip angles were usually 0° and 8° and the horizontal control settings were varied from 10° to -30°.

Forces and moments were measured with an internally mounted six-component strain-gage balance. The model was mounted on a movable support and driven through several angles of attack or sideslip during each run. The angles of attack and sideslip were set by using a prism mounted on the model to reflect light from a source onto a calibrated chart. The Mach number was obtained at each test point with a total-pressure probe located to avoid interference with the model bow shock. Regions on the model surface where separation, vortex scrubbing, or shock intersection occurred were

visualized by using an oil-flow technique. The model was painted black and a mixture of silicone oil and titanium dioxide was distributed in random dots over the model surface.

The estimated probable uncertainties in the force and moment coefficients were obtained by using the method of least squares. The accuracy of balance calibration, zero shift of balance during tests, computer readout, dynamic pressure, and pressure transducers were considered in estimating the probable uncertainties. These uncertainties are estimated to be within the following limits:

C_L	±0.004
C_D	±0.0007
L/D	±0.06
C_m	±0.0004
C_{l_β}	±0.0001
C_{n_β}	±0.0001
C_{Y_β}	±0.001

The accuracy of angle of attack and sideslip is estimated to be $\pm 0.10^\circ$ and of free-stream Mach number is estimated to be ±0.02.

The model base pressure was determined from the average of four measurements, and the axial force was adjusted to correspond to a base pressure equal to free-stream static pressure. Straight-line slopes between 0° and 4° sideslip were used to obtain the lateral stability parameters.

MODEL

The basic model was a 0.02-scale version of the M = 12 all-body research aircraft of references 1, 2, and 3. Sketches of model and component parts are shown in figure 1 and a photograph is shown in figure 2. The body had a delta planform with a 6.5° half-angle conical nose faired to an 80° swept leading edge afterbody. Aft of the conical nose the fuselage had modified rhombic cross sections with a fatness ratio A_{max}/S of 0.125.

The horizontal wing-tip-type control surfaces, vertical tails, and canards are shown in detail in figure 1(b). The horizontal control surfaces had a 70° leading-edge sweep, a diamond airfoil section, and a combined total exposed area of 9 percent of the body planform area. The horizontal controls were adjustable in 5° increments from $+15^\circ$ to -30°.

The vertical tails had a 77.8° swept upper edge and a 76.5° swept lower edge, a contoured airfoil section, and a combined total exposed area of 22 percent of the body planform area. The horizontal controls and vertical tails were removable so that the body could be tested alone. Contour blocks were used to fill in the leading edge of the body when it was tested without the controls. Two sets of canards with exposed surface areas of 2 percent and 4 percent of the body planform area were tested. The canards had a leading-edge sweep of 65° and symmetrical wedge airfoil sections. The model body was constructed of aluminum with a stainless-steel nose tip and control surfaces.

RESULTS AND DISCUSSION

Aerodynamic Characteristics

The effect of horizontal control deflections shown in figure 3 indicates that the aircraft (BHV) was longitudinally stable at Mach 6 for control deflection angles of 10° to -30° and angles of attack from -4° to 20°. The pitching-moment curves were nonlinear as were the lift curves, with lift-curve slope increasing with increasing angle of attack. As expected, C_L decreased with increased negative horizontal control settings and large control deflections caused large reductions in L/D. A maximum L/D of 3.5 occurred at $\delta_h = 0^\circ$ and $\alpha = 9.5^\circ$ (fig. 3), whereas a maximum trimmed L/D of 3.3 occurred at about $\alpha_{trim} = 11.5^\circ$ and $\delta_{h,trim} = -4^\circ$ (fig. 4). The trim deflection results in a decrease in L/D of 0.2 due to trim drag. An increase in the trimmed angle of attack from 0° to about 14° resulted in decreased stability as shown by the decrease in static margin in figure 4. The relatively constant slope of the $\delta_{h,trim}$ curve in figure 4 indicates that horizontal control effectiveness is about constant over the α range. As shown in figure 5, decreasing $R_{\infty,l}$ from 10.5×10^6 to 2.84×10^6 caused essentially no change in the longitudinal aerodynamic characteristics. A curve has been faired through the high Reynolds number data in figure 5.

The effect of the various components on the longitudinal characteristics is shown in figure 6. The body (B) was unstable. As expected, addition of the vertical tails to the body (BV) caused only a very slight change in stability, whereas the addition of the horizontal control surfaces resulted in a stable configuration (BHV). Addition of the smaller canards to the BHV configuration ($BHVC_S$) caused a reduction in stability to about neutral, and addition of the larger canards ($BHVC_B$) resulted in pitch-up moment above 8° angle of attack. The addition of various components caused compensating changes in C_L and C_D so that only small changes occurred in L/D. The vertical tails caused an increase in $C_{D,0}$ but had only a slight effect on drag due to lift and C_L, whereas the horizontal controls and canards caused increases in these parameters.

The effect of the various components on the lateral-directional aerodynamic characteristics is shown in figure 7. The body alone (B) was directionally unstable $\left(-C_{n_\beta}\right)$. The addition of the vertical tails (BV) caused a large increase in stability to about neutral, and addition of the horizontal controls (BHV) caused only a slight change in directional stability. Addition of canards to the configuration resulted in an increase in directional stability. This was probably due to a reduction in the high-pressure region near the nose by the separated and vortex flow regions aft of the canards as shown in the oil-flow photographs discussed later. The body alone (B) had positive effective dihedral $\left(-C_{l_\beta}\right)$ above an angle of attack of 2°. The addition of vertical control surfaces (BV) and canards $\left(\text{BHVC}_S \text{ and } \text{BHVC}_B\right)$ caused essentially no change in lateral stability, whereas addition of the horizontal controls (BHV) increased the positive effective dihedral at $\alpha > 2^\circ$.

As shown in figure 8, the yawing and rolling of the BHV configuration were slightly nonlinear at $\beta > 4^\circ$ and $\alpha = 9.87^\circ$ and both directional and lateral stability were reduced at $\delta_h = -5^\circ$. This variation with β may be due to impingement of the bow shock on the horizontal control surface which occurred at $\beta = 4^\circ$ or due to the asymmetric vortex flow on the lee surface. (See discussion of oil-flow studies.) The longitudinal aerodynamic characteristics did not change between $\beta = 0^\circ$ and 4° (fig. 9).

Only small to moderate changes occurred in most of the aircraft trimmed characteristics as a result of vertical movement of the center of gravity which may occur as fuel is consumed during flight. However, $(L/D)_{trim}$ did change substantially at $\delta_h = 0^\circ$ and 5° (fig. 10). At these control deflections the aircraft trims along the steeply rising part of the L/D curve so that relatively small changes in trim angle result in substantial changes in $(L/D)_{trim}$. Propellant-tank location and propellant sequencing were selected to insure that the longitudinal center-of-gravity location remained within aerodynamic limits at all times.

Comparison With Theory

The computer program described in references 5 and 6 was used to compute the theoretical aerodynamic characteristics. The program calculates and sums both the viscous and inviscid forces acting on the aircraft. Computer drawings showing the shape and location of surface elements for the computations are shown in figure 11. A number of hypersonic theories were used to determine the pressure forces in compression regions. The theories used were tangent cone, tangent wedge, modified Newtonian, two-dimensional shock expansion, and Dahlem-Buck empirical. The latter empirical method approximates tangent-cone pressures at low impact angles and approaches Newtonian values at high impact angles. In the expansion regions either two-dimensional shock-expansion theory or Prandtl-Meyer theory was used to compute the pressure forces. Free-stream conditions were used ahead of each component. The skin friction was computed by using the

reference-temperature method for the laminar boundary layer and Spalding-Chi theory for the turbulent boundary layer. A brief discussion of the theories is given in reference 5.

A turbulent boundary layer existed over most of the model surface (BHV) at the higher Reynolds number (ref. 7) and therefore was used in the computer calculations. The effect of neglecting the short initial laminar boundary layer can be estimated from figure 12, which is a comparison of the calculated aerodynamic characteristics for completely laminar and turbulent boundary layers. There is a maximum difference of about 20 percent in C_D and L/D and no difference in C_L and C_m. The effect of unknown model wall temperature is shown in figure 13. Varying the model wall temperature from 311 K to 478 K did not significantly change any of the calculated coefficients.

The tangent-cone approximation with free-stream conditions ahead of the body generally gave the best agreement with the longitudinal data for the HYFAC body (fig. 14), but tended to depart from the data at the higher angles of attack and underestimated the positive pitching moment. As can be seen in figure 15, the tangent-cone method gave good agreement with the lateral-directional data for the body (B).

Figure 16 shows a comparison of a number of hypersonic theories with the longitudinal aerodynamic data for the BHV configuration over the range of control deflections and angle of attack. Use of the tangent-cone method for all components gave the best general agreement (fig. 16), but as can be seen in figure 17, only within a range approximated by control deflections between 5° and -5°, and positive values of C_L less than about 0.17. This range includes the trim angle for maximum $(L/D)_{trim}$ (fig. 4), and the tangent-cone theory gave good agreement with the trim characteristics near maximum $(L/D)_{trim}$. The closer agreement with pitching moment for the BHV configuration as compared with the body alone (B) (fig. 14) must be the result of compensating differences.

A comparison of the hypersonic theories with the lateral-directional stability data for the BHV configuration in figure 18 indicates that use of the tangent-cone method for the vertical tail gave the best general agreement. In this comparison the tangent-cone method was used for the body and horizontal controls and the method used for the vertical tails was varied. The directional stability was overestimated for the BHV configuration as compared with the good agreement for the body alone (fig. 15), but good agreement was obtained in C_{l_β} and C_{Y_β} for both configurations.

The increasing disagreement between the theories and the data at large negative control settings was probably due in part to the use of free-stream conditions ahead of the controls instead of the local dynamic pressure. An estimate of the local conditions ahead of the horizontal controls at small deflections and zero angle of attack obtained by using conical shocks and Prandtl-Meyer expansions did indicate a return to close to free-

stream conditions ahead of the controls in agreement with the previous comparisons, but attempts to estimate local conditions at angles of attack and large control deflections were unsuccessful. Additional factors which could influence the flow over the horizontal controls include determination of a more accurate shock shape, the change in shock shape and flow field with angle of attack, unporting of the controls from the body, and the effect of flow separation on the control surface. Such a detailed analysis is beyond the scope of the present study.

Comparison With Other Data

Complete configurations.- It is of interest to compare the hypersonic aerodynamic characteristics of the HYFAC configuration with those of an all-body aircraft tested by Ames Research Center and reported in reference 8. This configuration has an elliptical-cone forebody and an afterbody with elliptical cross sections. The dimensions of this model are shown in figure 19. The following table gives a comparison of the test conditions and geometry of the models. It is believed that the difference in Mach number and Reynolds number does not significantly alter the comparison.

	HYFAC	Elliptical-cross-section configuration
M_∞	6.00	5.37 (longitudinal characteristics) 7.30 (lateral-directional characteristics)
$R_{\infty,l}$	2.84×10^6 and 10.5×10^6	3.95×10^6
S, cm^2	318.13	[a]690.14
l, cm	48.11	48.26
b, cm	12.52	25.86
A_{max}/S	0.125	0.0935
Λ, deg	83.5 and 80	75
Exposed planform area:		
Horizontal tail	0.09S	0.125S
Vertical tail	0.22S	0.169S
Canards	0.04S	0.04S

[a]Reference area has been increased 10 percent to make comparable with HYFAC area which includes the horizontal tail.

Figure 20 shows a comparison of the longitudinal aerodynamic characteristics of the two aircraft (BHV). The $C_{D,o}$ of the two configurations was about the same. The elliptical configuration (ref. 8) had a considerably larger C_{L_α}, probably due to its lower leading-edge sweep, so that in spite of greater drag due to lift, the elliptical configuration had an $(L/D)_{max}$ of about 4.0 as compared with 3.5 for the HYFAC. With a center-of-gravity location of $0.64l$ the elliptical configuration had almost neutral stability and might be difficult to trim to $(L/D)_{max}$, whereas the HYFAC was stable and could be trimmed over the range of angle of attack. As shown in figure 21, the addition of canards $(BHVC_B)$ with an exposed planform area of 4 percent of the reference area caused a reduction in stability for both configurations to about neutral or caused pitch-up, depending on angle of attack.

Both configurations (BHV) had close to neutral directional stability, and the elliptical configuration had greater lateral stability (C_l) at $\alpha = 4.8^o$ as can be seen in figure 22. The lateral stability of HYFAC increased with angle of attack and was greater at $\alpha = 10^o$ $\left(\text{near maximum } (L/D)_{trim}\right)$ than the elliptical configuration was at $\alpha = 4.8^o$.

Body-alone data.- The following table gives a comparison of the geometry and test conditions for the HYFAC body (B_1) and several elliptical bodies (B_1, B_2, and B_3) reported in reference 9. Of the bodies listed in the table, B_1 was the body of the elliptical-cross-section aircraft discussed previously, B_2 had the lowest value of A_{max}/S and the highest $(L/D)_{max}$ of the four bodies tested in reference 9, and B_3 was an alternate sweep model.

	HYFAC	B_1	B_2	B_3
M_∞	6.0	5.37	5.37	5.37 (longitudinal characteristics)
		7.38	7.38	7.38 (lateral-directional characteristics)
$R_{\infty,l}$	2.84×10^6 10.5×10^6	3.95×10^6	4.52×10^6	4.54×10^6
S, cm^2	318.13	[a]690.14	[a]902.78	[a]600.41
l, cm	48.11	48.26	55.19	55.48
b,cm	12.52	25.86	29.58	19.57
Λ, deg	83.5 and 80	75	75	80
A_{max}/S	0.125	0.0935	0.0625	0.0935

[a]Reference areas have been increased 10 percent to make comparable with HYFAC area which includes the horizontal tails.

The HYFAC body (B) had about the same $C_{D,o}$ as configuration B_1 (fig. 23). Apparently the larger frontal area of the HYFAC with an A_{max}/S of 0.125 as compared with 0.0935 for B_1 is offset by skin friction, leading-edge bluntness, and base drag. Decreasing the fatness ratio to 0.0625 more than compensated for these factors so that B_2 had a considerably lower $C_{D,o}$. The HYFAC had less drag due to lift, but a considerably smaller C_{L_α} than B_1 and B_2 which as a consequence had higher values of $(L/D)_{max}$. Configurations B_1 and B_2 had pitch-up moments with a center-of-gravity location at $0.64l$ whereas the HYFAC body had about neutral stability.

As can be seen in figure 24, the HYFAC, B_1, and B_3 had about neutral lateral stability. Also, B_1 and B_3 had about neutral directional stability whereas the HYFAC body was unstable.

OIL-FLOW STUDIES

The variation in the HYFAC surface flow patterns with angle of attack is shown in the top three photographs of figures 25(a), 25(b), and 25(c). The upper surface is shown in figure 25(a), the fuselage side in figure 25(b), and the lower surface in figure 25(c). At $\alpha = 0^\circ$, a region of separated flow occurred in a triangular region on the upper surface at the aft end (fig. 25(a)) and in a small region on the lower surface of the nose (fig. 25(c)). The region between the vertical tails on the lower surface may also be separated. At $\alpha = 10^\circ$, the flow separated along the 80° swept leading edge and reattached in a short distance with the "feather" type of scrubbing pattern of a vortex flow which extended along the fuselage upper side to the rear of the model (figs. 25(a) and 25(b)). A vortex also occurred on the lee side along the center line from the nose to the end of the model. The region on the windward surface between the vertical tails at $\alpha = 10^\circ$ shows a distinct V-shaped pattern due either to tail-fuselage interference or three-dimensional separation. Similar vortex flows occurred at $\alpha = 16^\circ$, but it appears that the leading-edge flow may remain separated for a longer distance before reattachment with a shorter region of vortex scrubbing (figs. 25(a) and 25(b)). At angles of attack of 0°, 10°, and 16°, parallel surface flow occurred on the lower surface in regions where a scramjet inlet could be located (fig 25(c)). Note the effect of the difference in horizontal tail deflection on the oil-flow patterns.

The fourth photograph from the top in figure 25 shows the asymmetric flow field which occurred at 4° of sideslip at $\alpha = 10^\circ$. On the lee side (fig. 25(a)), the center-line vortex is skewed, the vortex flow due to separation along the windward leading edge has moved inboard and is reduced in size, and the vortex due to separation along the opposite leading edge is smaller.

The fifth photograph from the top in figure 25(a) shows the effect of canards $BHVC_S$ at $\alpha = 10^{\circ}$. Canards caused both the leading-edge flow separation and vortex patterns to extend forward to the base of the canards (figs. 25(a) and 25(b)). The canards also altered the lower surface flow (fig. 25(c)).

The regions of vortex flow shown in the oil-flow studies may contain hot spots and experience considerably higher heating rates (ref. 10). Heat protection systems will need to take into account the existence and movement of the hot spots with angle of attack, sideslip, and roll.

CONCLUDING REMARKS

An investigation has been conducted to determine the hypersonic aerodynamic characteristics of an all-body, delta-planform, hypersonic research aircraft (HYFAC configuration). Tests were conducted at Mach 6, at Reynolds numbers based on model length of 2.84×10^6 and 10.5×10^6, over an angle-of-attack range from -4° to 20° and an angle-of-sideslip range from 0° to 8°, and at horizontal control deflections from 10° to -30°. The wind-tunnel results show that the HYFAC configuration is longitudinally stable and can be trimmed over the range of test conditions. A maximum trimmed lift-drag ratio of 3.3 occurred at a horizontal control deflection of about -4° and angle of attack of 11.5°. The aircraft had a small degree of positive directional stability over the angle-of-attack range and positive effective dihedral at angles of attack greater than 2°. Addition of canards caused a decrease in longitudinal stability and an increase in directional stability.

A limited comparison of the wind-tunnel data with several hypersonic approximations showed that except for directional stability the tangent-cone method gave the best agreement at control settings between 5° and -5° and at positive values of lift coefficient. None of the methods adequately predicted the longitudinal characteristics at negative lift coefficients and large negative control deflections.

A limited comparison indicates that the HYFAC configuration has greater longitudinal stability than elliptical-cross-section configurations but lower maximum lift-drag ratio.

Oil-flow studies revealed extensive areas of separated and vortex flow on the fuselage lee surface which varied in extent and location with angle of attack and sideslip. Canards caused additional areas of vortex flow.

Langley Research Center,
National Aeronautics and Space Administration,
Hampton, Va., October 10, 1973.

REFERENCES

1. Anon.: Hypersonic Research Facilities Study. Phase I – Preliminary Studies. Vol. II, Pt. 2 – Flight Vehicle Synthesis. MDC A0013 (Contract No. NAS2-5458), McDonnell Aircraft Co., Oct. 2, 1970. (Available as NASA CR-114324.)

2. Anon.: Hypersonic Research Facilities Study. Phase II – Parametric Studies. Vol. III, Pt. 2 – Flight Vehicle Synthesis. MDC A0013 (Contract No. NAS2-5458), McDonnell Aircraft Co., Oct. 2, 1970. (Available as NASA CR-114326.)

3. Anon.: Hypersonic Research Facilities Study. Phase III – Final Studies. Vol. IV, Pt. 1 – Flight Research Facilities. MDC A0013 (Contract No. NAS2-5458), McDonnell Aircraft Co., Oct. 2, 1970. (Available as NASA CR-114327.)

4. Goldberg, Theodore J.; and Hefner, Jerry N. (With appendix by James C. Emery): Starting Phenomena for Hypersonic Inlets With Thick Turbulent Boundary Layers at Mach 6. NASA TN D-6280, 1971.

5. Gentry, Arvel E.: Hypersonic Arbitrary-Body Aerodynamic Computer Program (Mark III Version). Vol. I – User's Manual. Rep. DAC 61552, Vol. I (Air Force Contract Nos. F33615 67 C 1008 and F33615 67 C 1602), McDonnell Douglas Corp., Apr. 1968. (Available from DDC as AD 851 811.)

6. Gentry, Arvel E.; and Smythe, Douglas N.: Hypersonic Arbitrary-Body Aerodynamic Computer Program (Mark III Version). Vol. II – Program Formulation and Listings. Rep. DAC 61552, Vol. II (Air Force Contract Nos. F33615 67 C 1008 and F33615 67 C 1602), McDonnell Douglas Corp., Apr. 1968. (Available from DDC as AD 851 812.)

7. Goldberg, Theodore J.; Hefner, Jerry N.; and Stone, David R.: Hypersonic Aerodynamic Characteristics of Two Delta-Wing X-15 Airplane Configurations. NASA TN D-5498, 1969.

8. Nelms, Walter P., Jr.; and Thomas, Charles L.: Aerodynamic Characteristics of an All-Body Hypersonic Aircraft Configuration at Mach Numbers From 0.65 to 10.6. NASA TN D-6577, 1971.

9. Nelms, Walter P., Jr.: Effects of Body Shape on the Aerodynamic Characteristics of an All-Body Hypersonic Aircraft Configuration at Mach Numbers From 0.65 to 10.6. NASA TN D-6821, 1972.

10. Hefner, Jerry N.; and Whitehead, Allen H., Jr.: Lee-Side Heating Investigations. Part I – Experimental Lee-Side Heating Studies on a Delta-Wing Orbiter. NASA Space Shuttle Technology Conference, NASA TM X-2272, 1971, pp. 267-287.

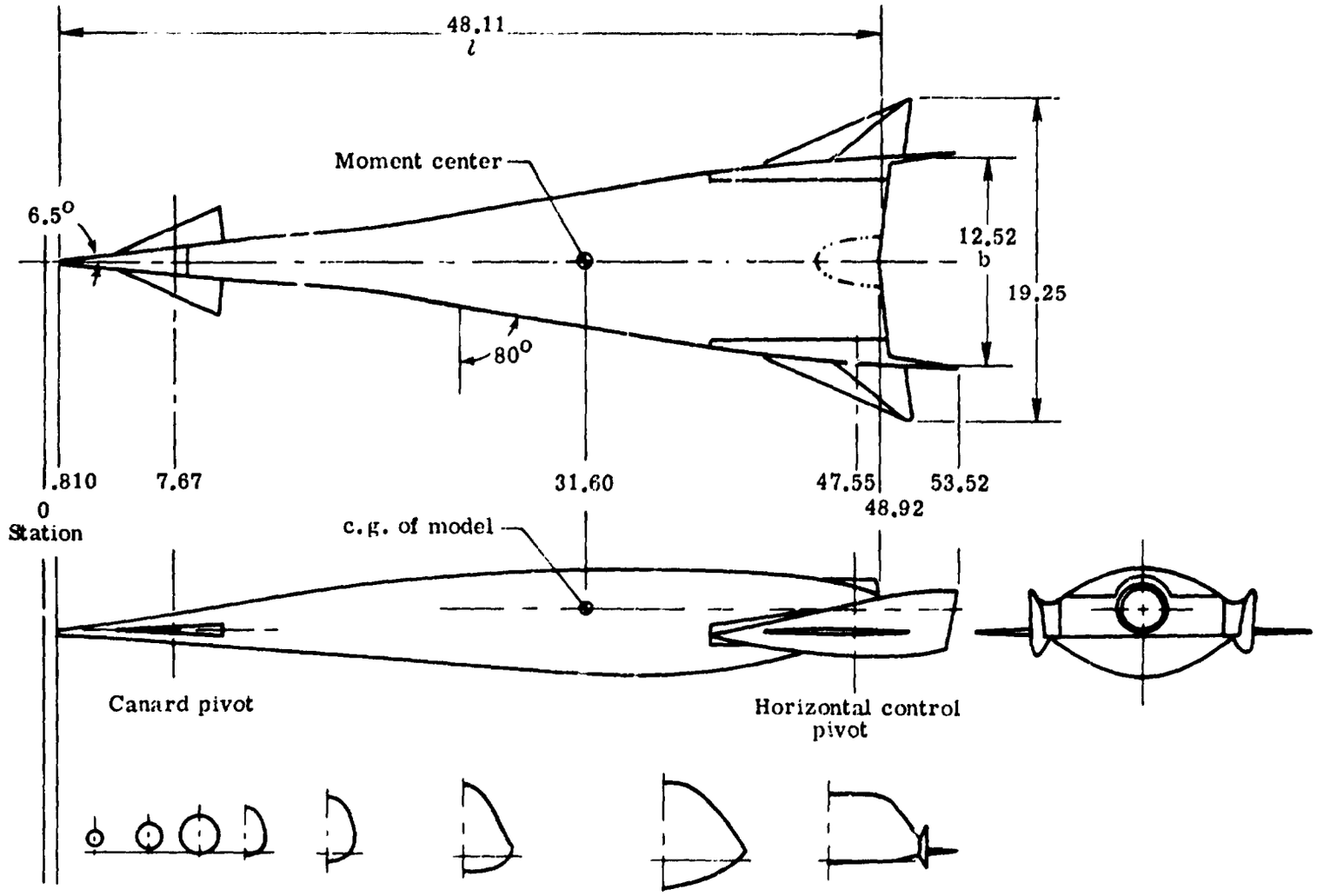

(a) $BHVC_B$.

Figure 1.- HYFAC model. All dimensions in centimeters.

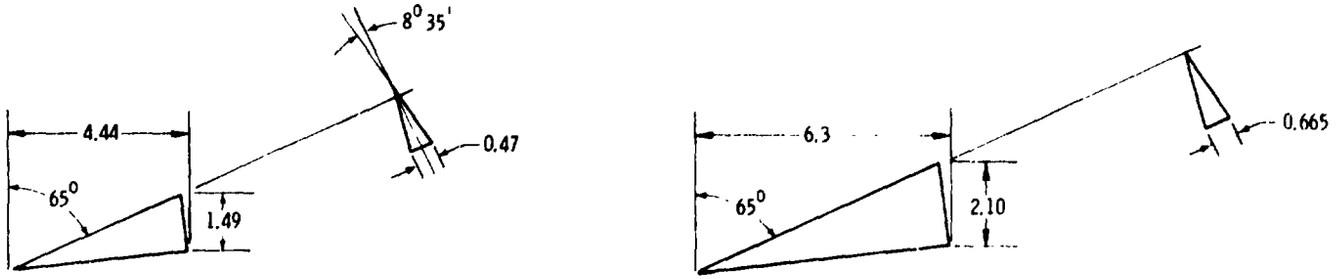

Canards

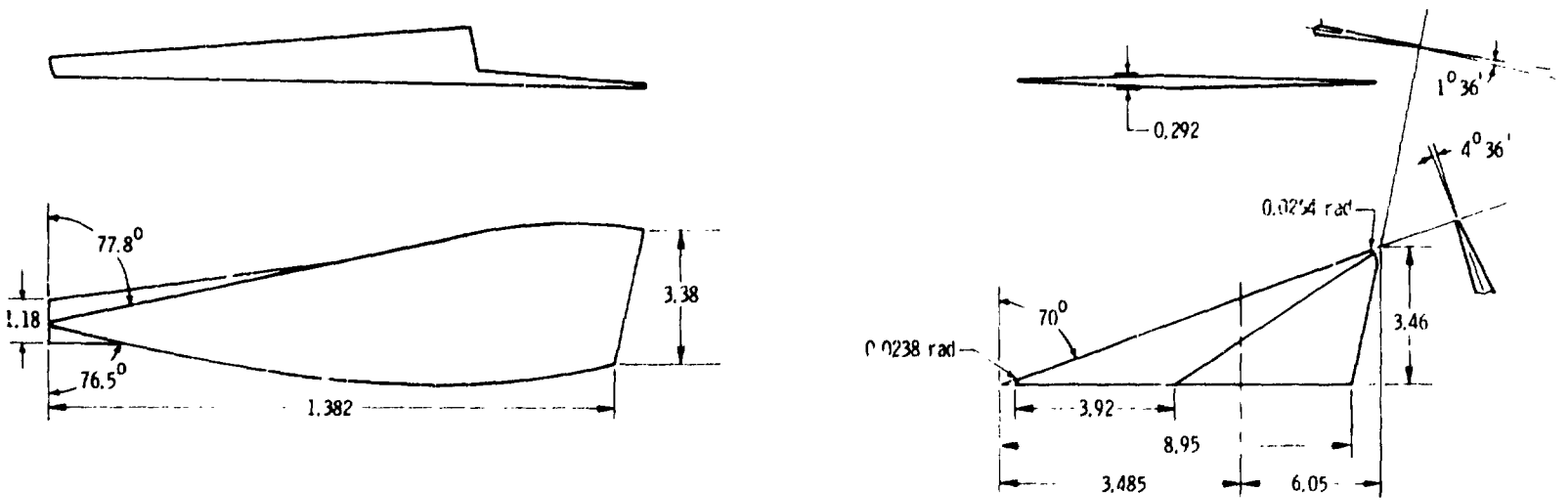

Vertical tail

Horizontal control surface

(b) Components.

Figure 1.- Concluded.

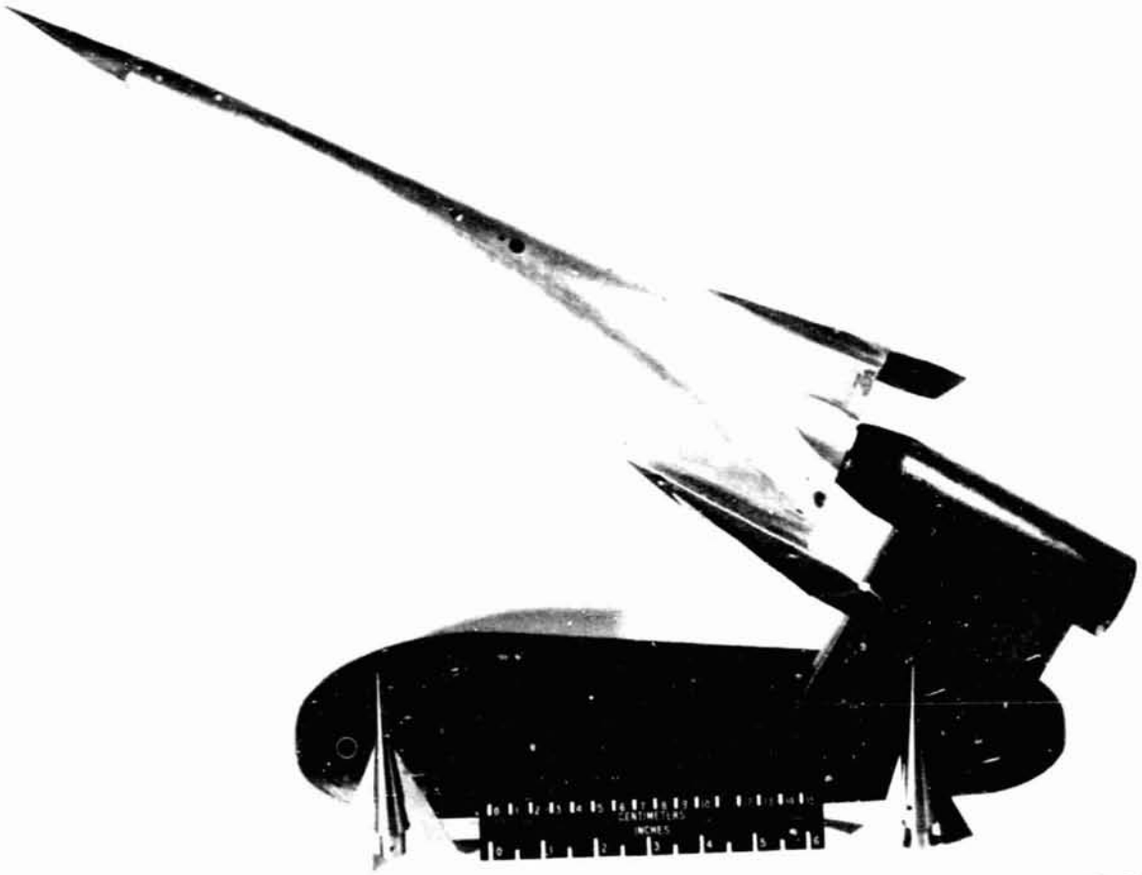

L-73-823

Figure 2.- HYFAC model, BHV.

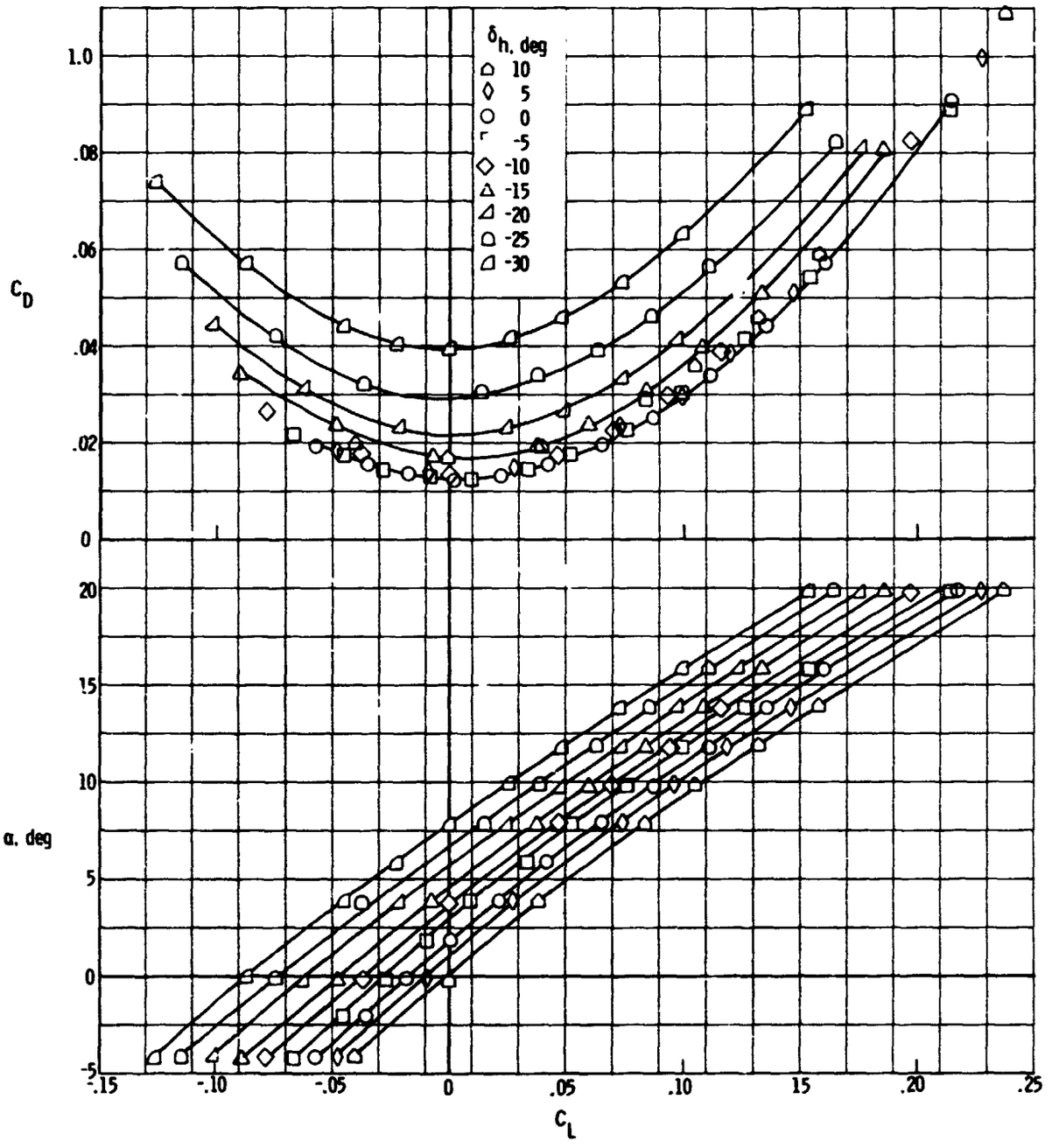

Figure 3.- Effect of horizontal stabilizer deflection on longitudinal aerodynamic characteristics. $R_{\infty,l} = 10.5 \times 10^6$; BHV.

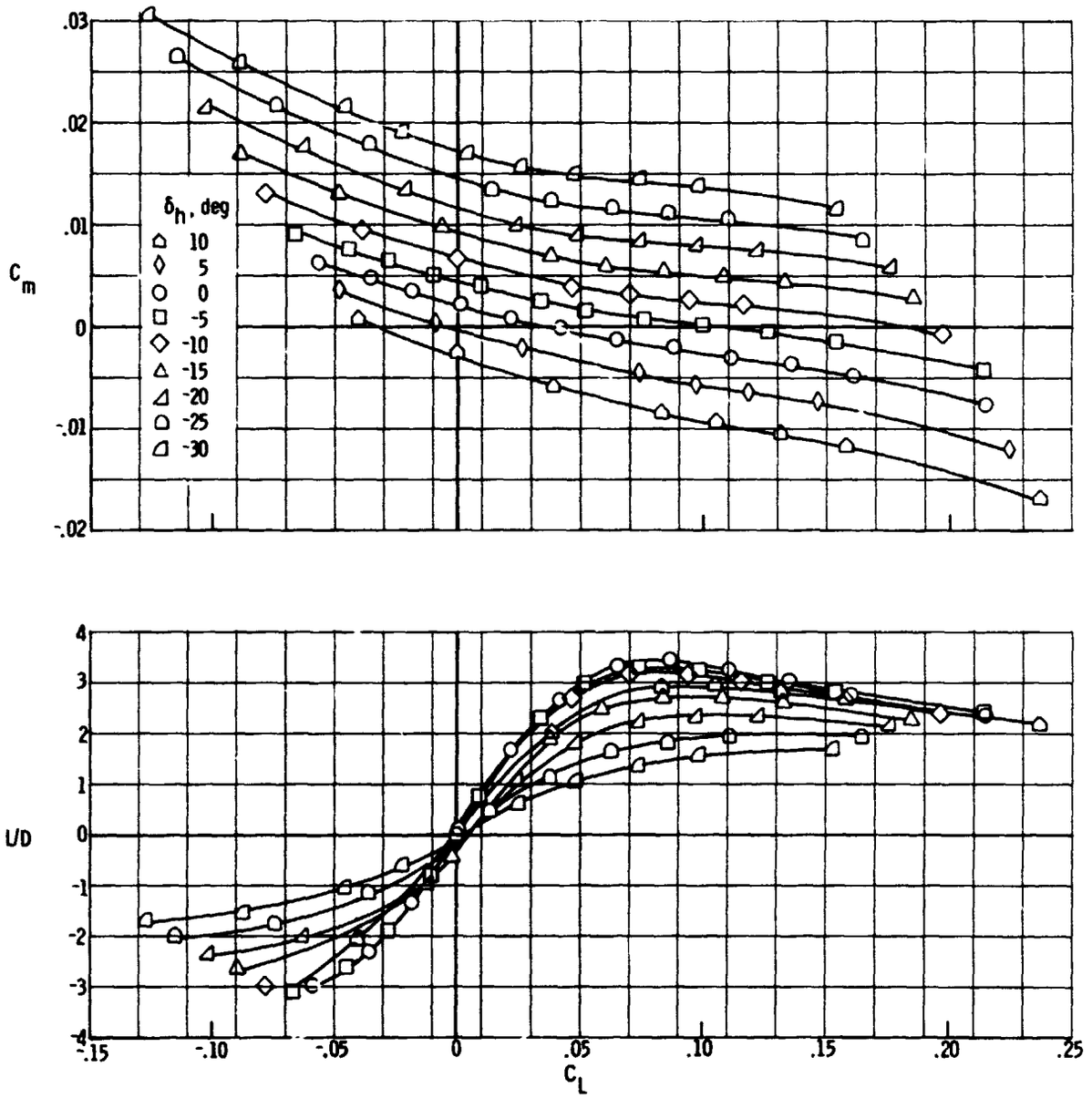

Figure 3.- Concluded.

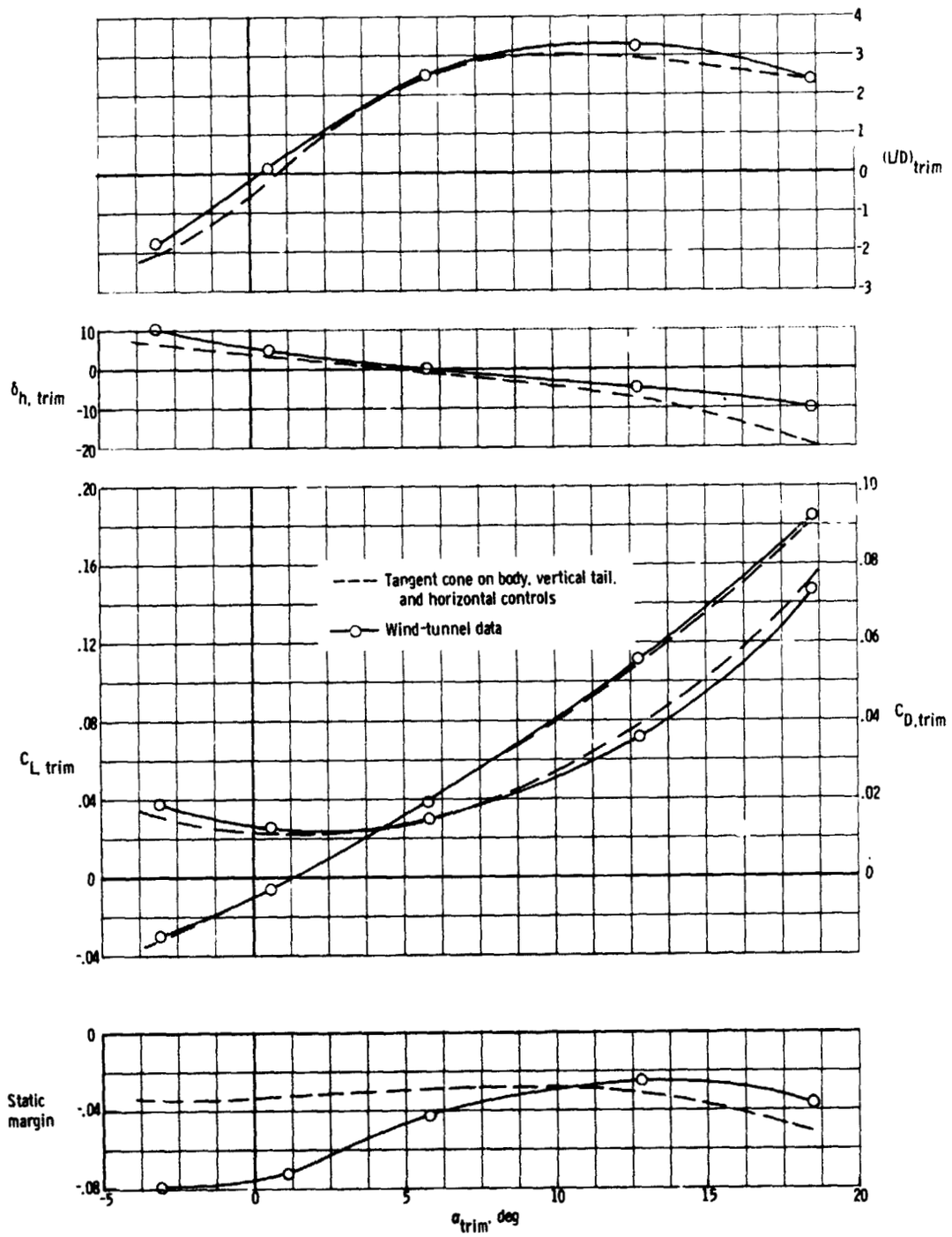

Figure 4.- Longitudinal trim characteristics. $R_{\infty,l} = 10.5 \times 10^6$; BHV.

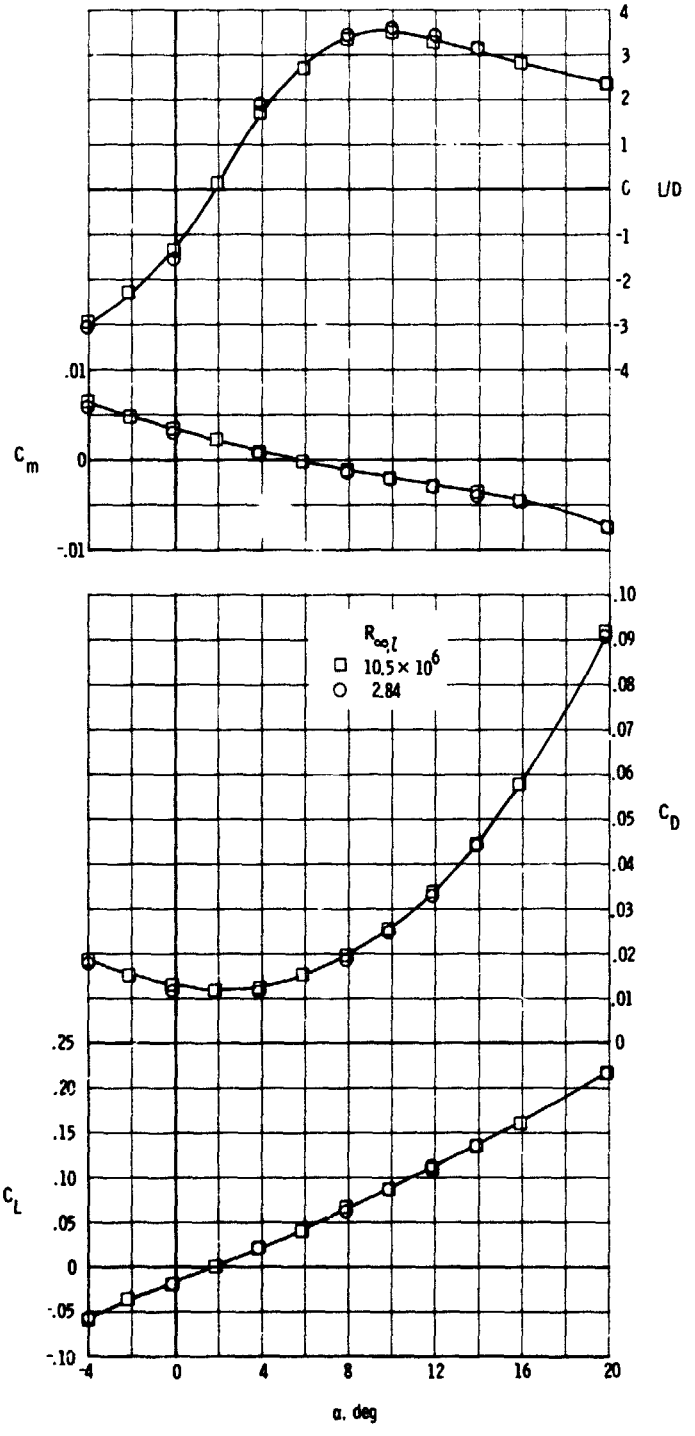

Figure 5.- Effect of Reynolds number on longitudinal aerodynamic characteristics. $\delta_h = 0^o$; BHV.

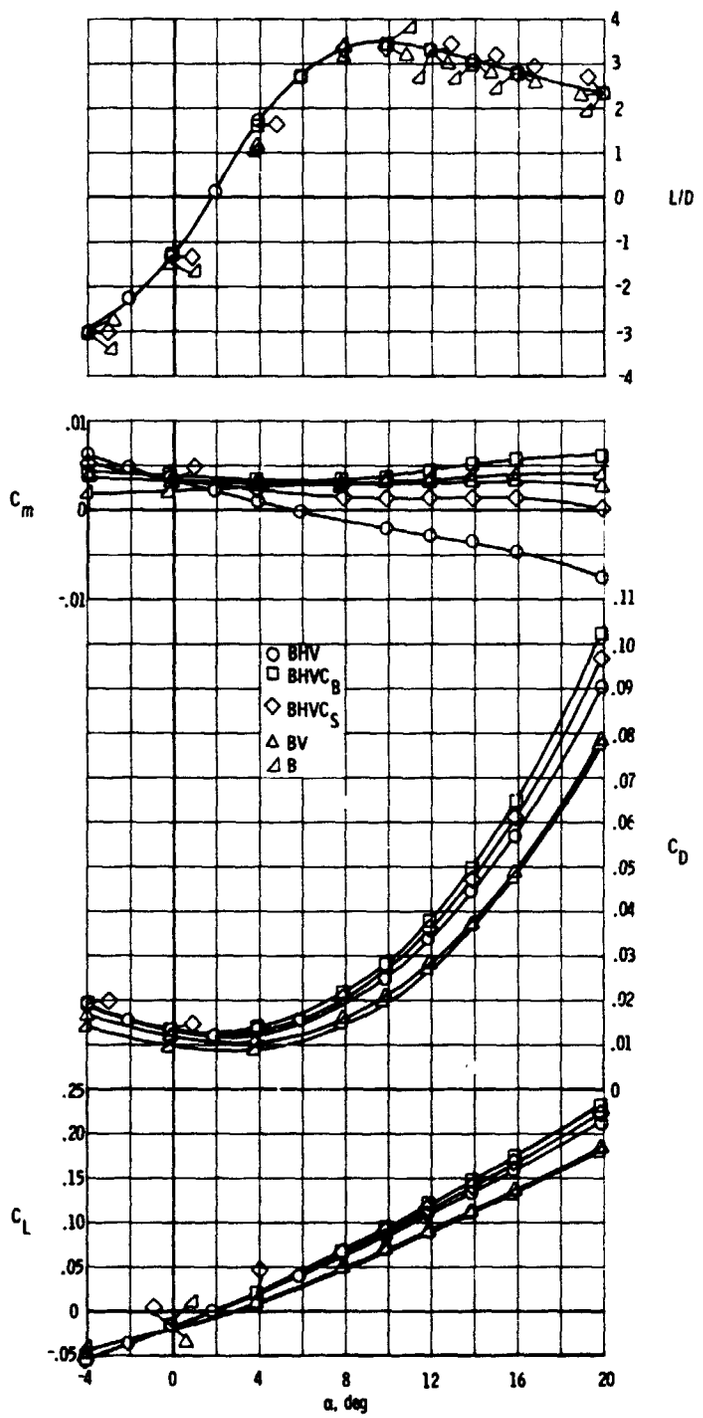

Figure 6.- Effect of various components on longitudinal aerodynamic characteristics. $R_{\infty,\ell} = 10.5 \times 10^6$; $\delta_h = 0^o$; $\delta_c = 0^o$.

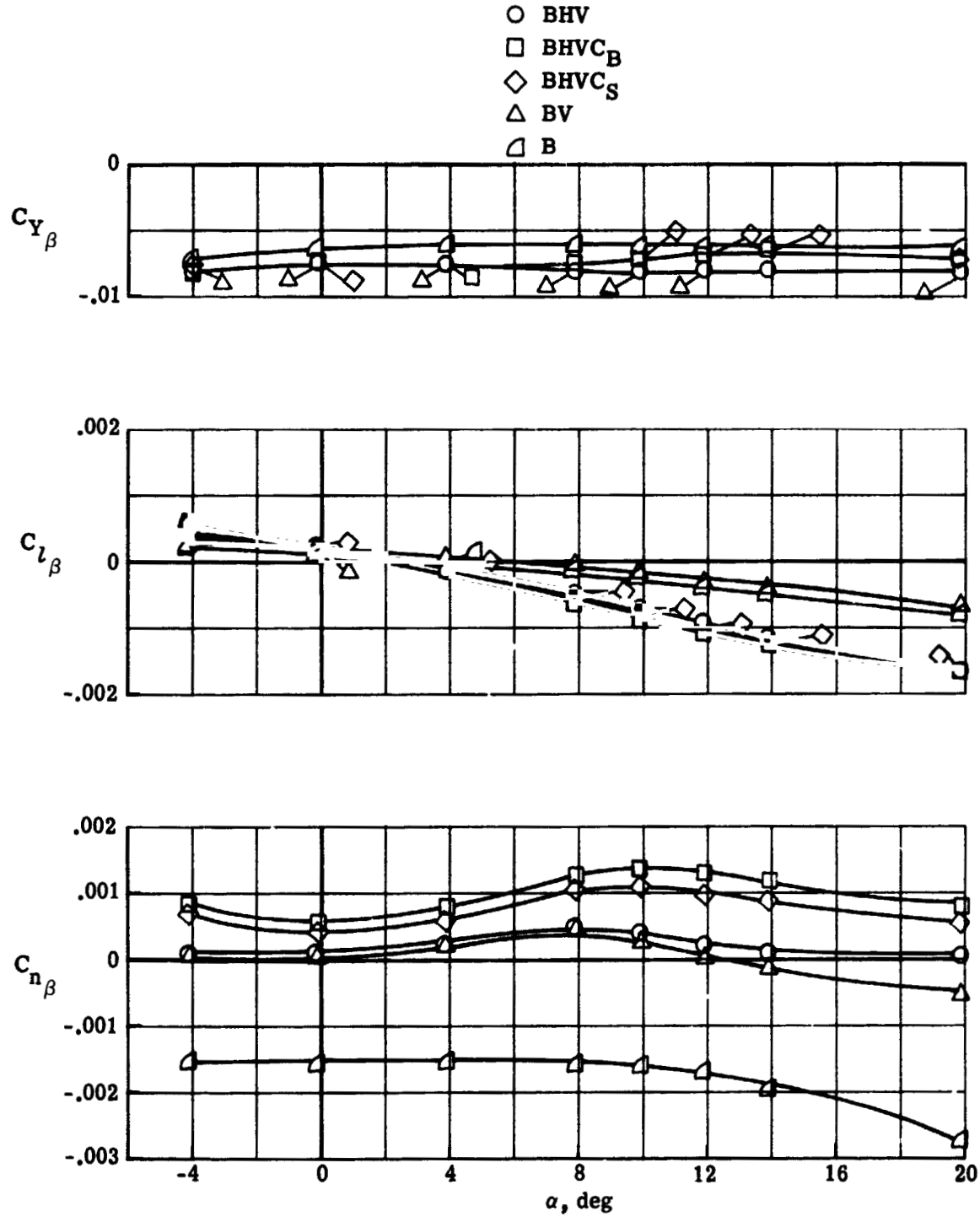

Figure 7.- Effect of various components on lateral-directional aerodynamic characteristics. $R_{\infty,\ell} = 10.5 \times 10^6$; $\delta_h = 0^o$; $\delta_c = 0^o$.

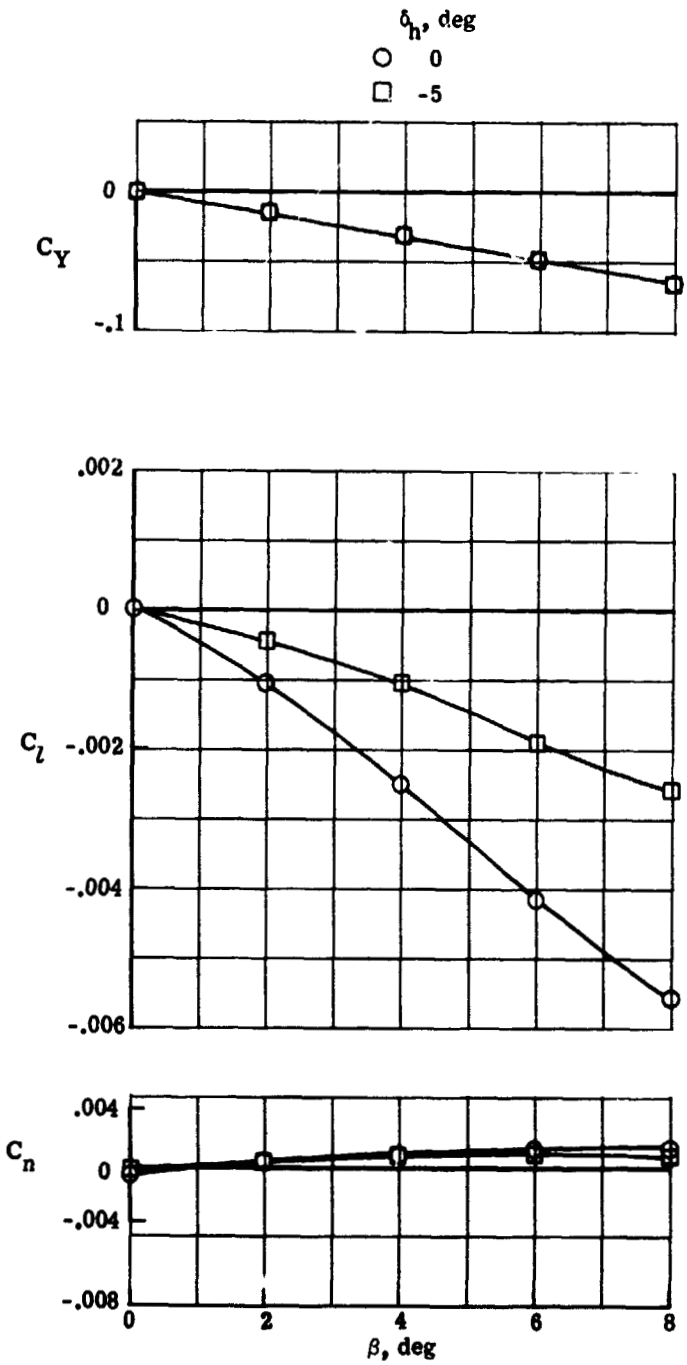

Figure 8.- Variation of lateral-directional stability with β. $\alpha = 9.87^{\circ}$; $R_{\infty,l} = 10.5 \times 10^6$; BHV.

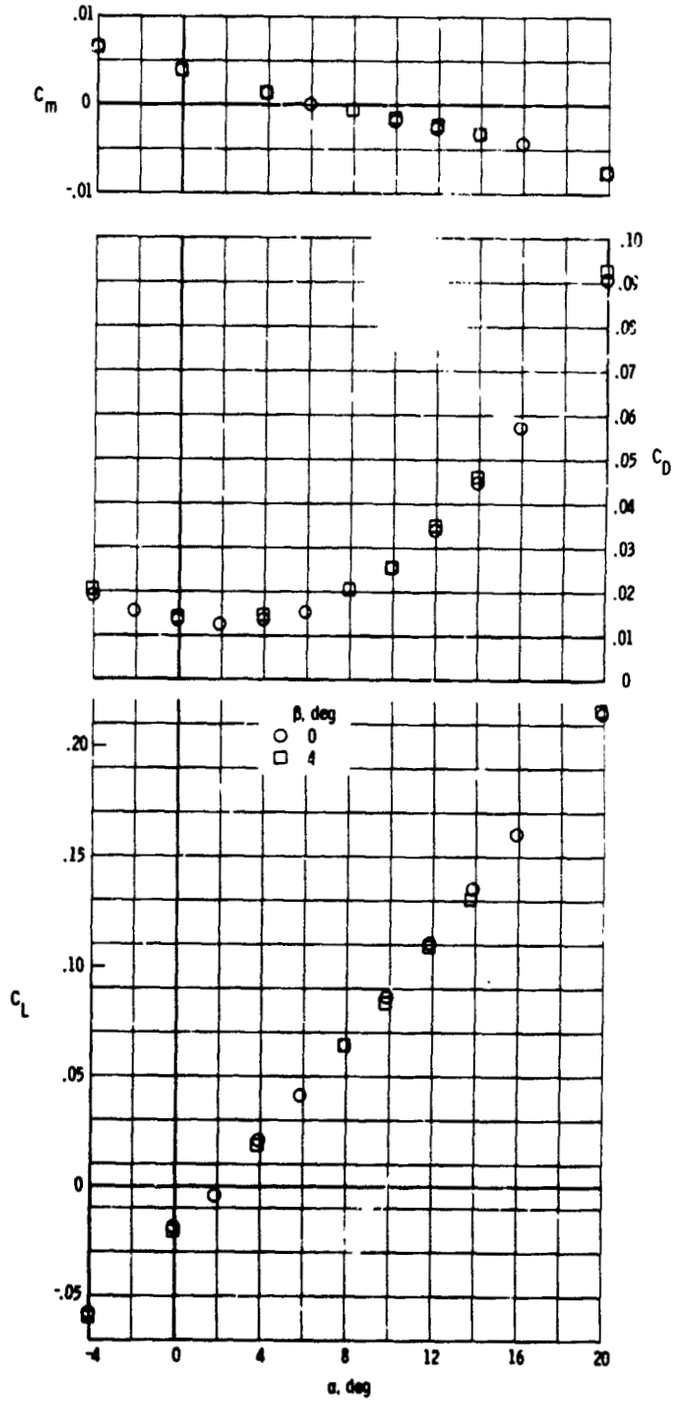

Figure 9.- Effect of β on longitudinal aerodynamic characteristics. $R_{\infty,\ell} = 10.5 \times 10^6$; BHV; $\delta_h = 0^o$.

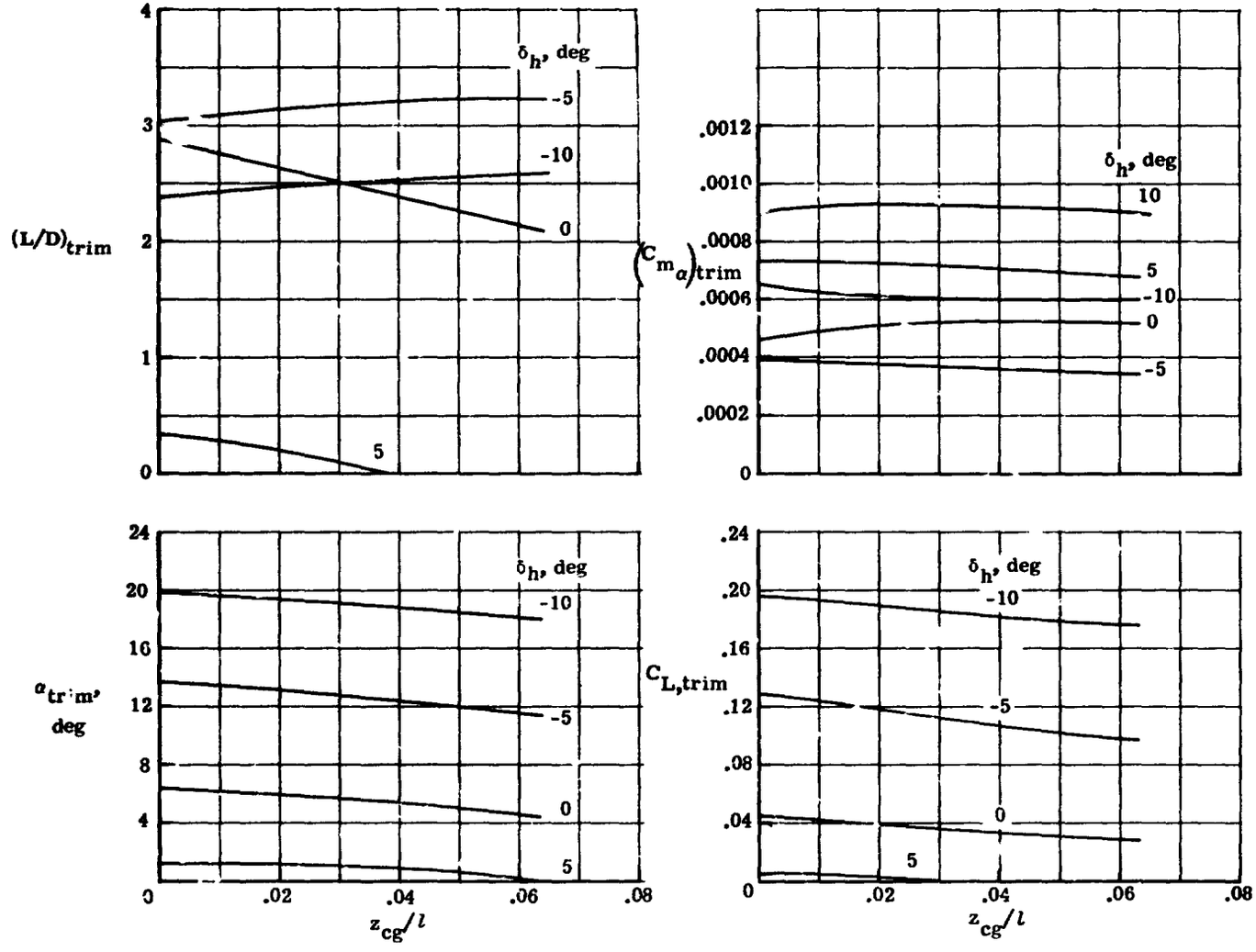

Figure 10.- Effect of variation in z_{cg} on trim characteristics for BHV.

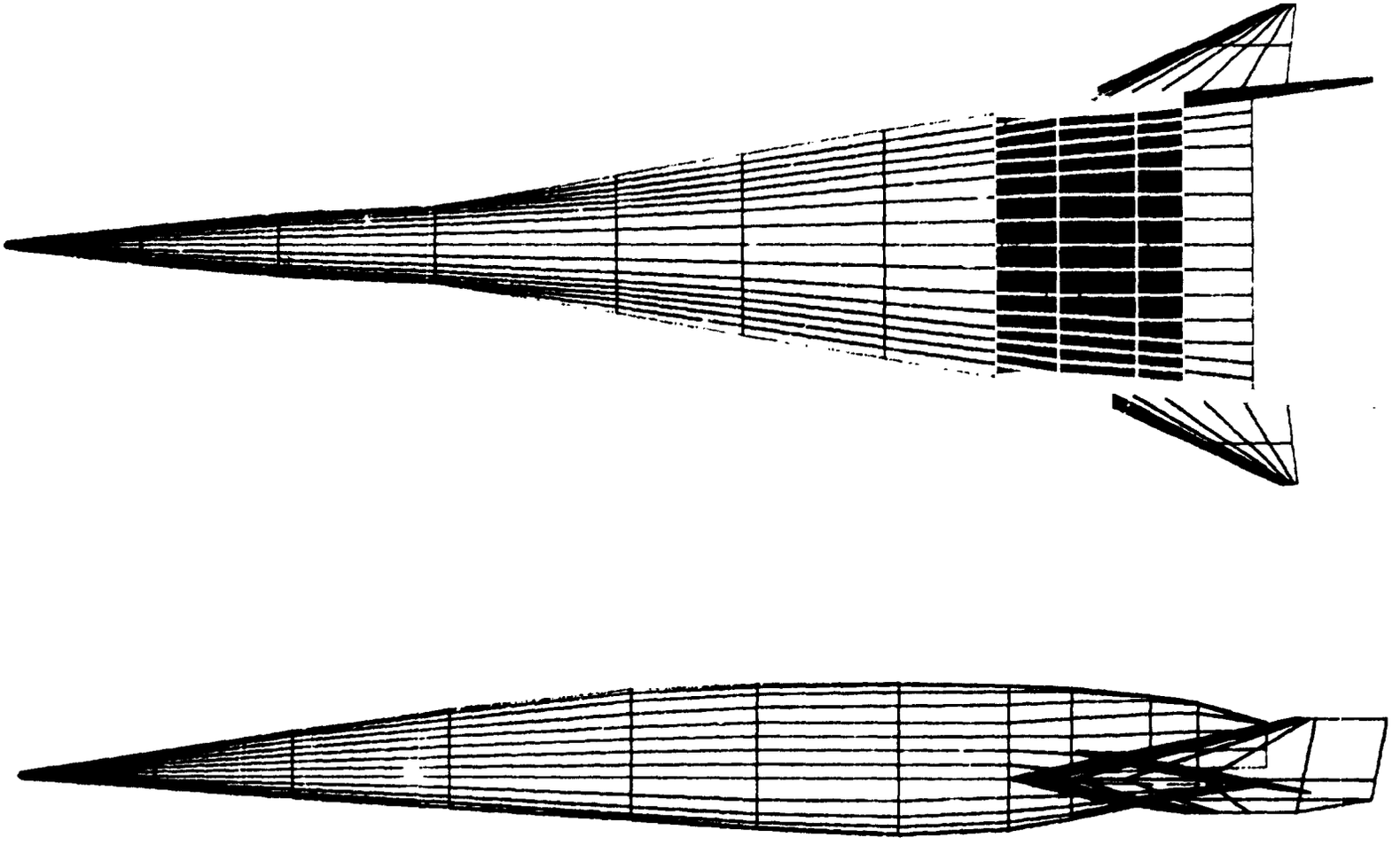

Figure 11.- Computer drawings of input geometry for BHV.

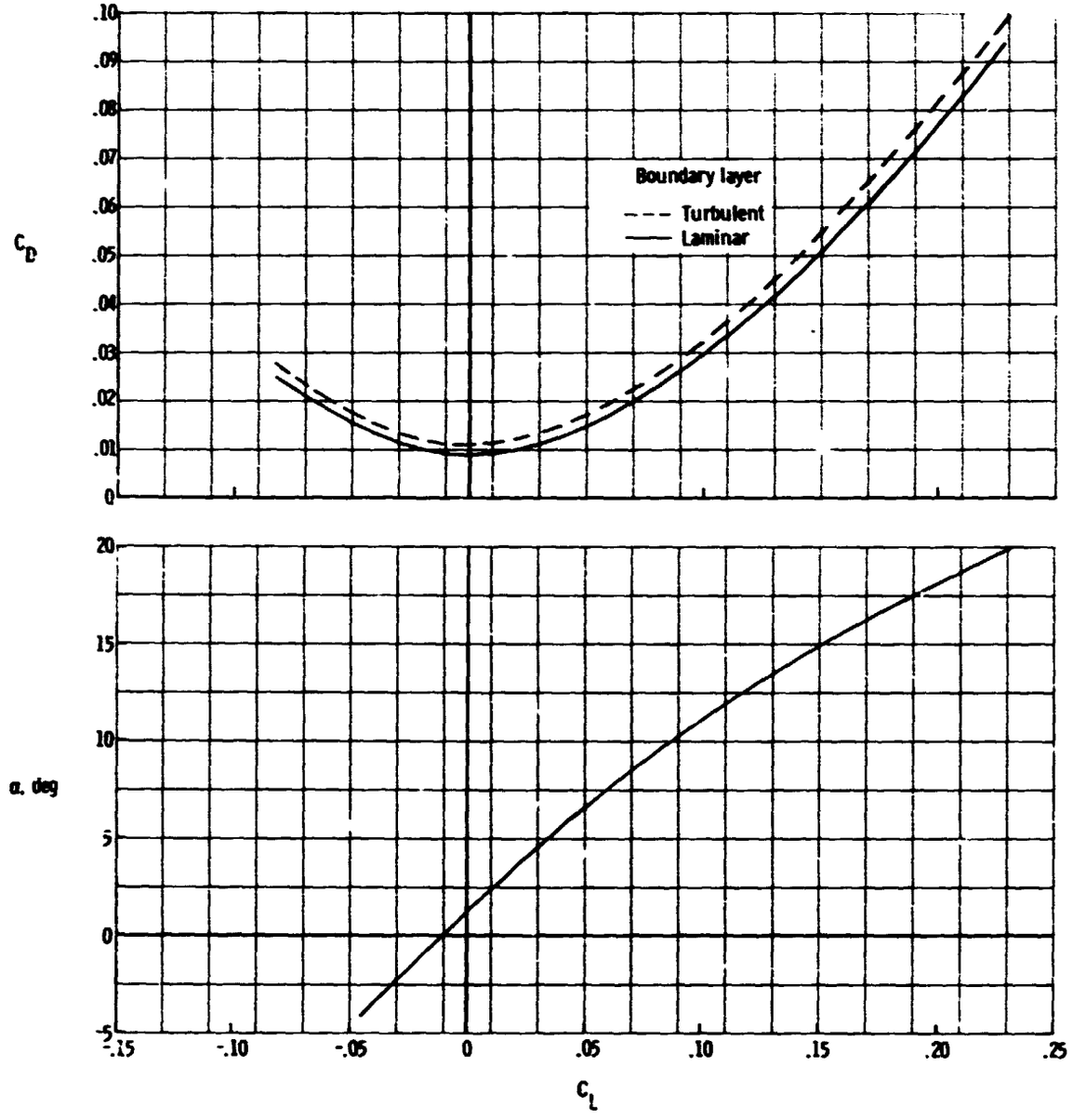

Figure 12.- Effect of boundary-layer state on theoretical longitudinal aerodynamic characteristics. $R_{\infty,\ell} = 10.5 \times 10^6$; BHV; $\delta_h = 0^o$.

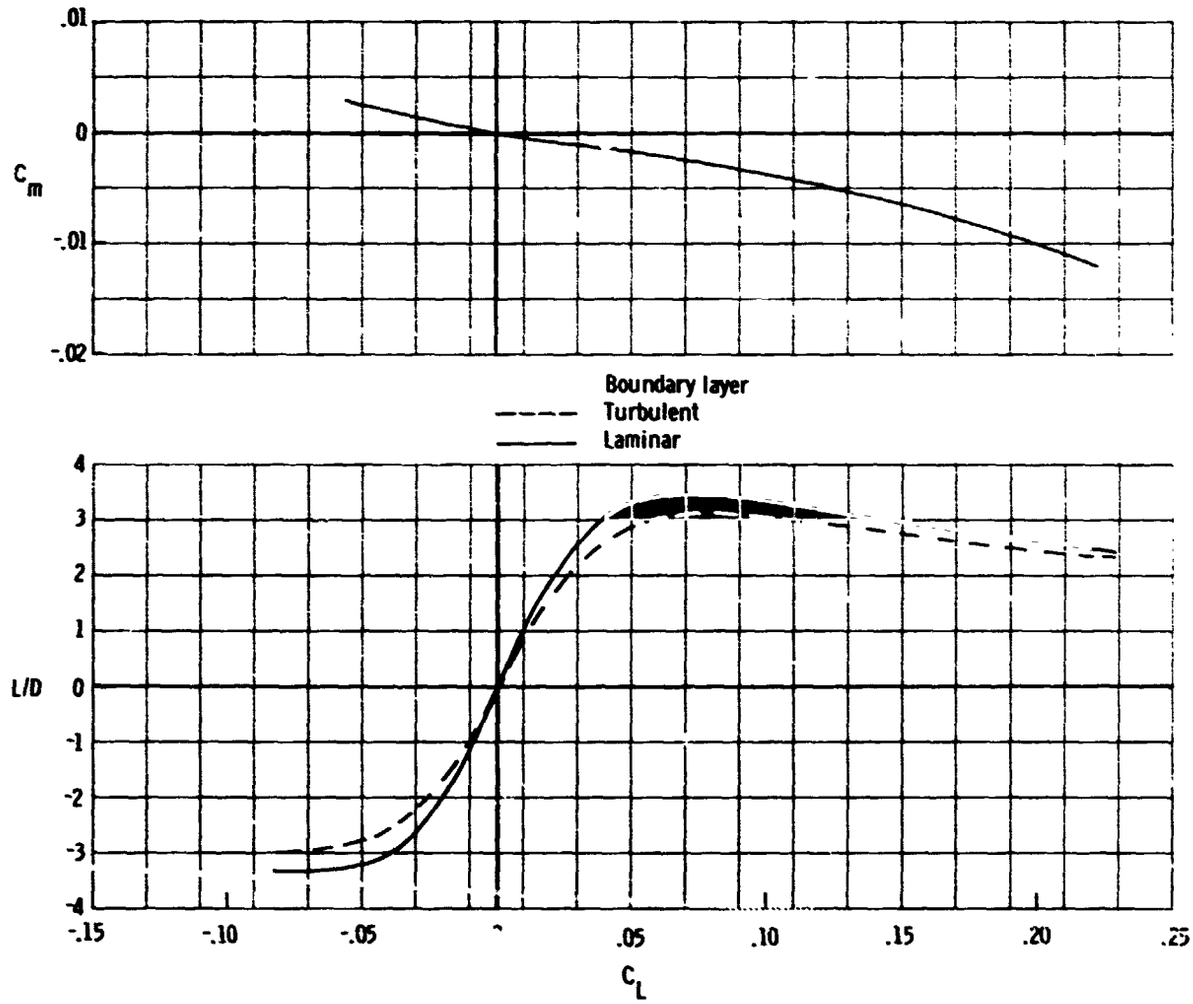

Figure 12.- Concluded.

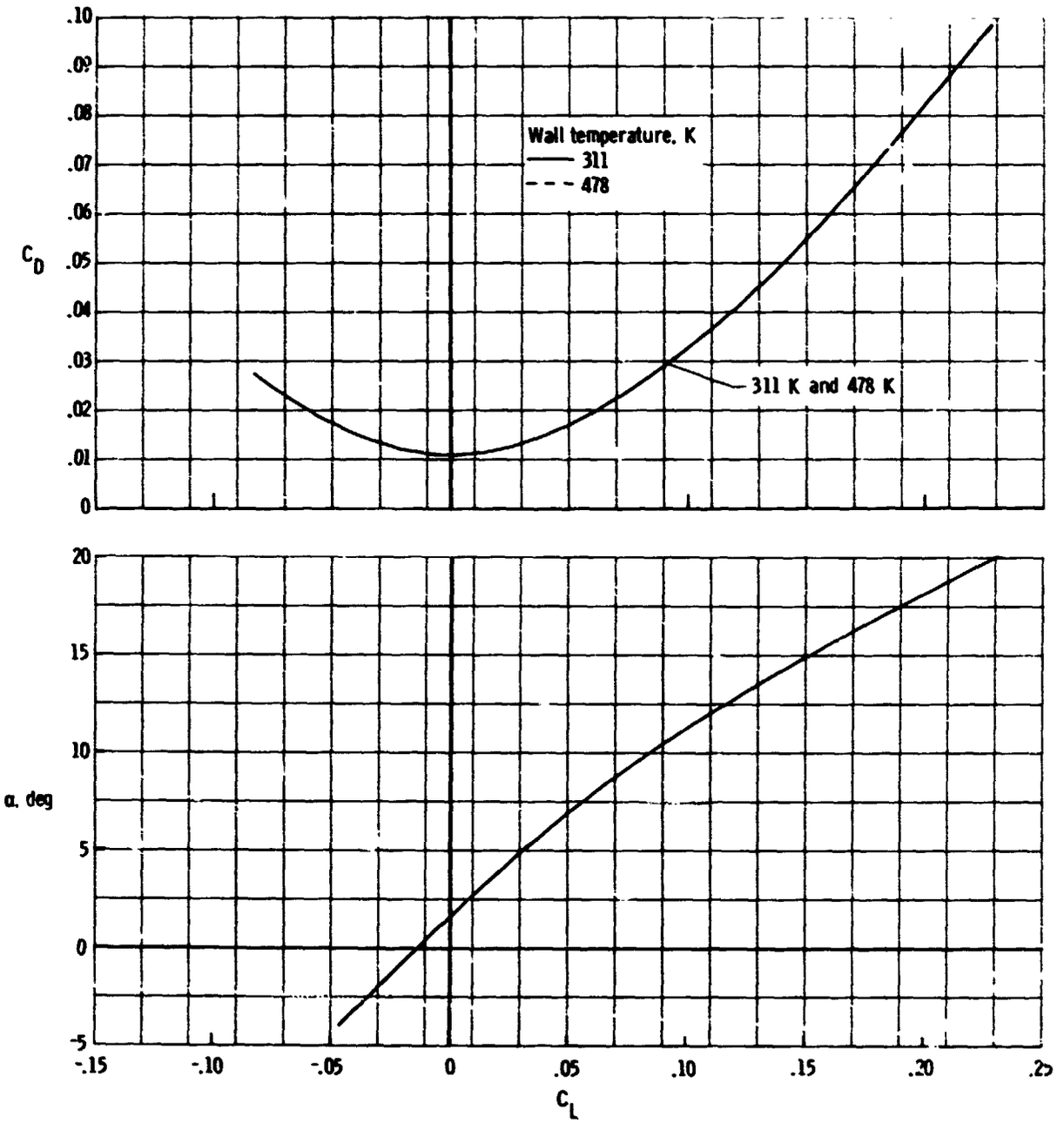

Figure 13.- Effect of wall temperature on theoretical longitudinal aerodynamic characteristics. Turbulent boundary layer; $R_{\infty,l} = 10\,5 \times 10^6$; BHV; $\delta_h = 0^o$.

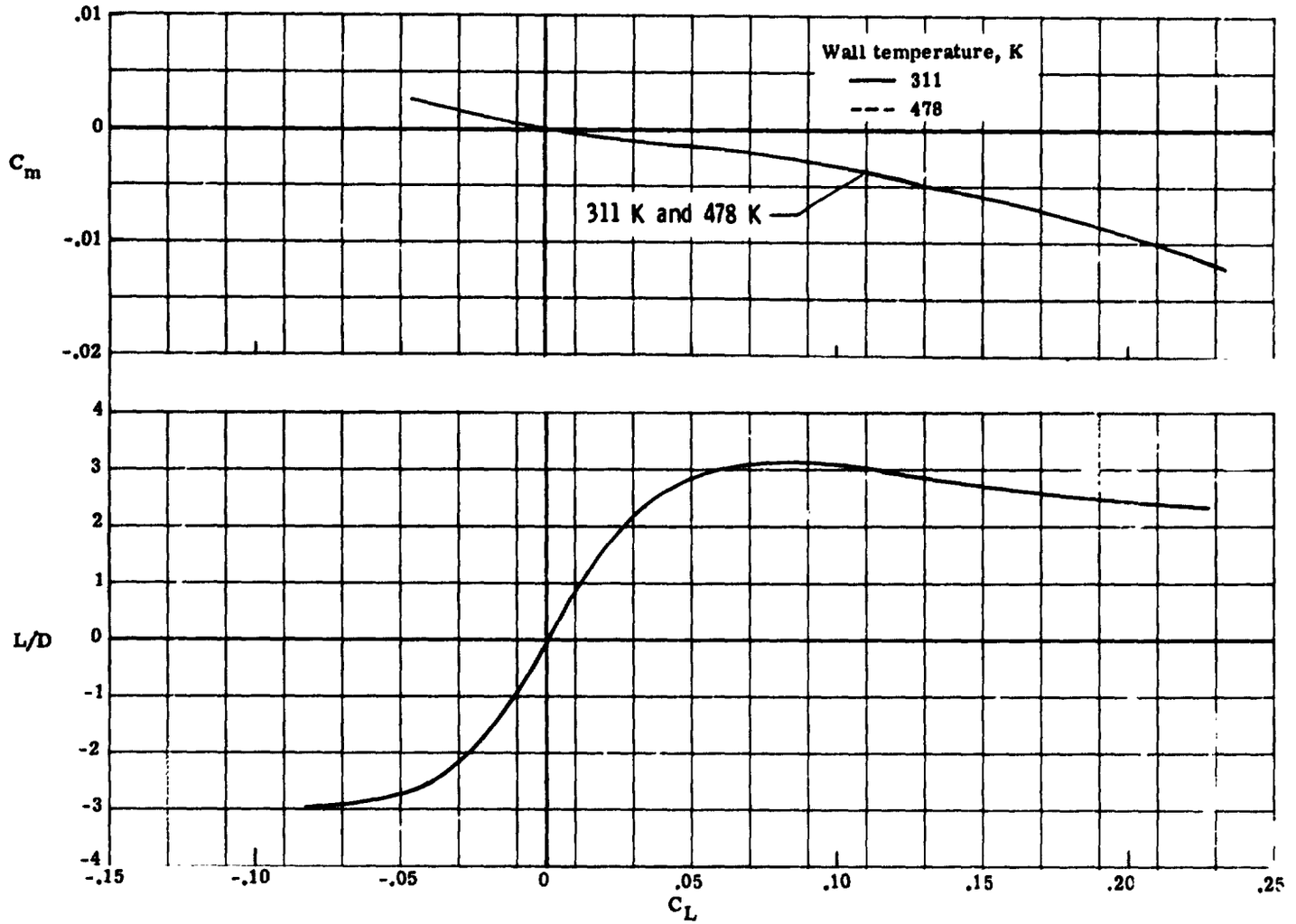

Figure 13.- Concluded.

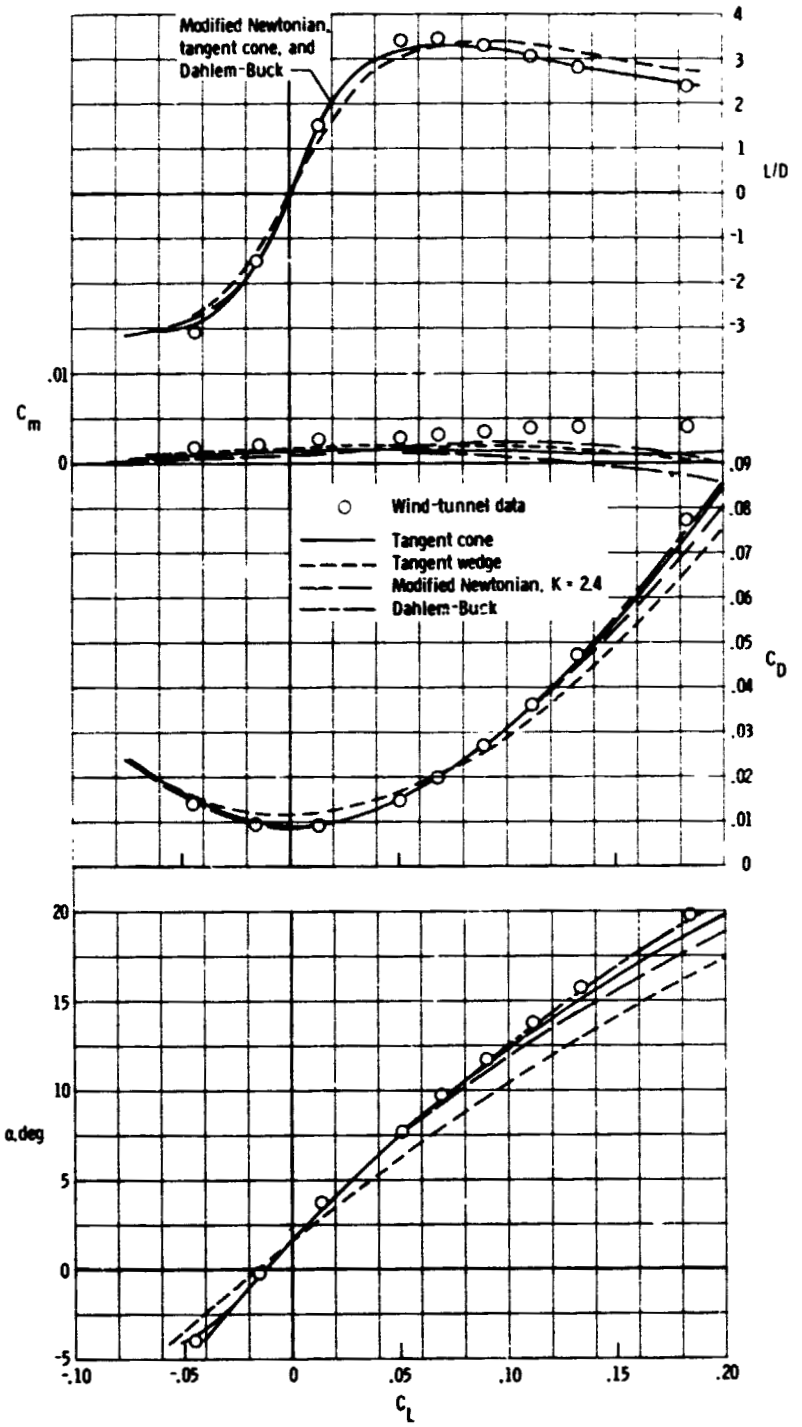

Figure 14.- Comparison of several hypersonic theories with wind-tunnel data for HYFAC body (B).

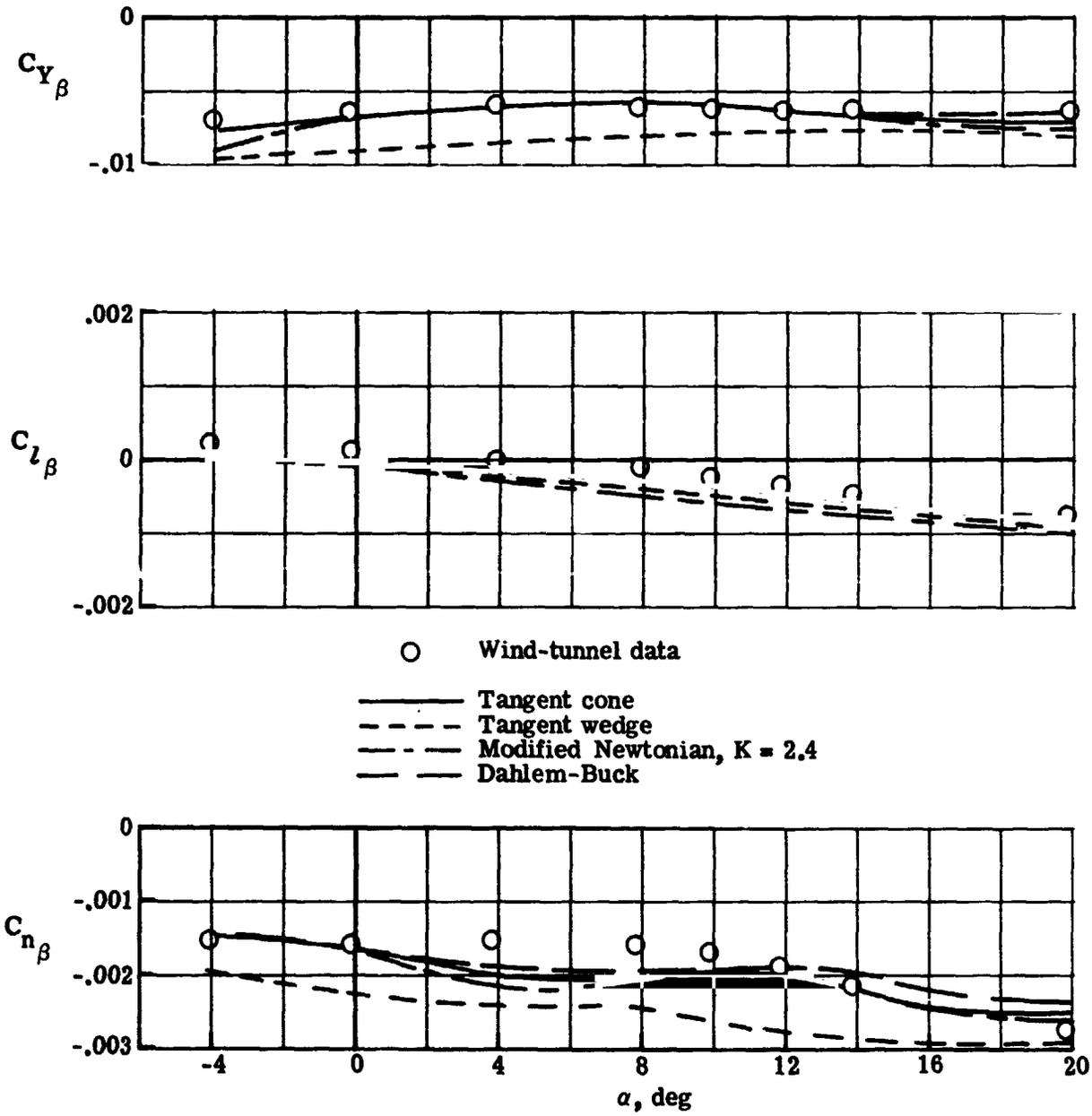

Figure 15.- Comparison of several theories with wind-tunnel data for lateral-directional stability characteristics of HYFAC body (B) at $R_{\infty,l} = 10.5 \times 10^6$.

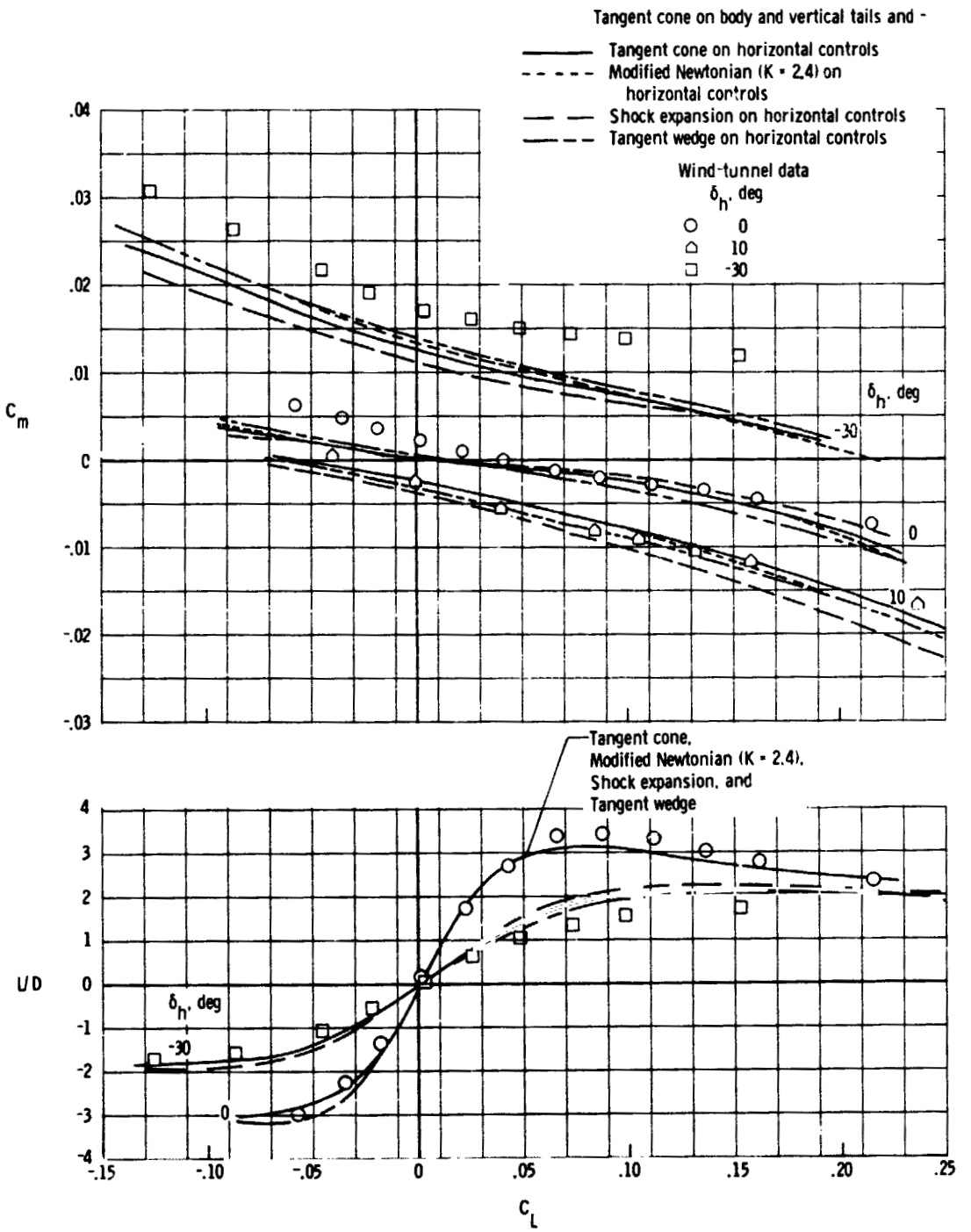

Figure 16.- Comparison of several hypersonic theories with wind-tunnel data for HYFAC configuration (BHV) at $R_{\infty,l} = 10.5 \times 10^6$.

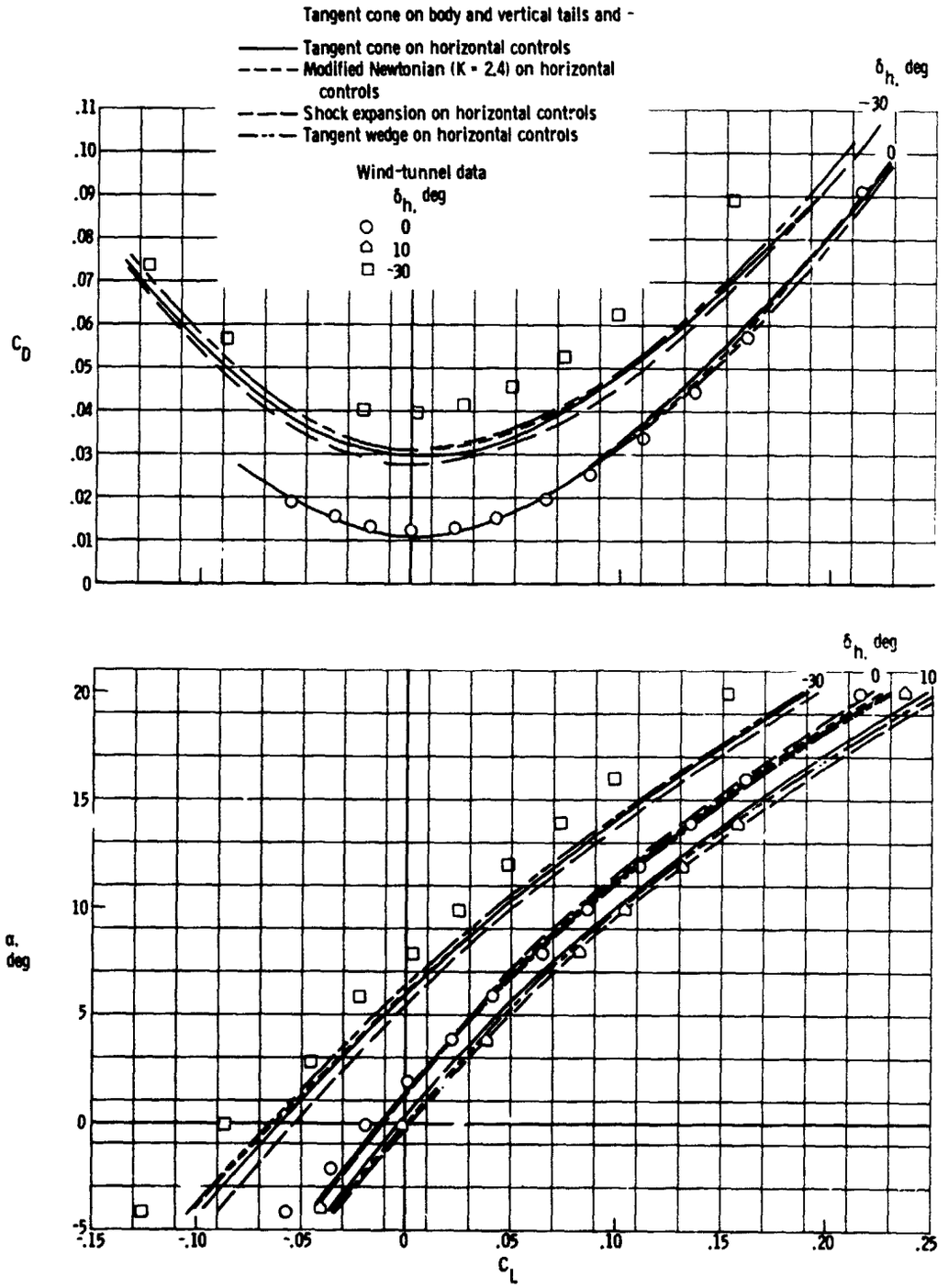

Figure 16.- Concluded.

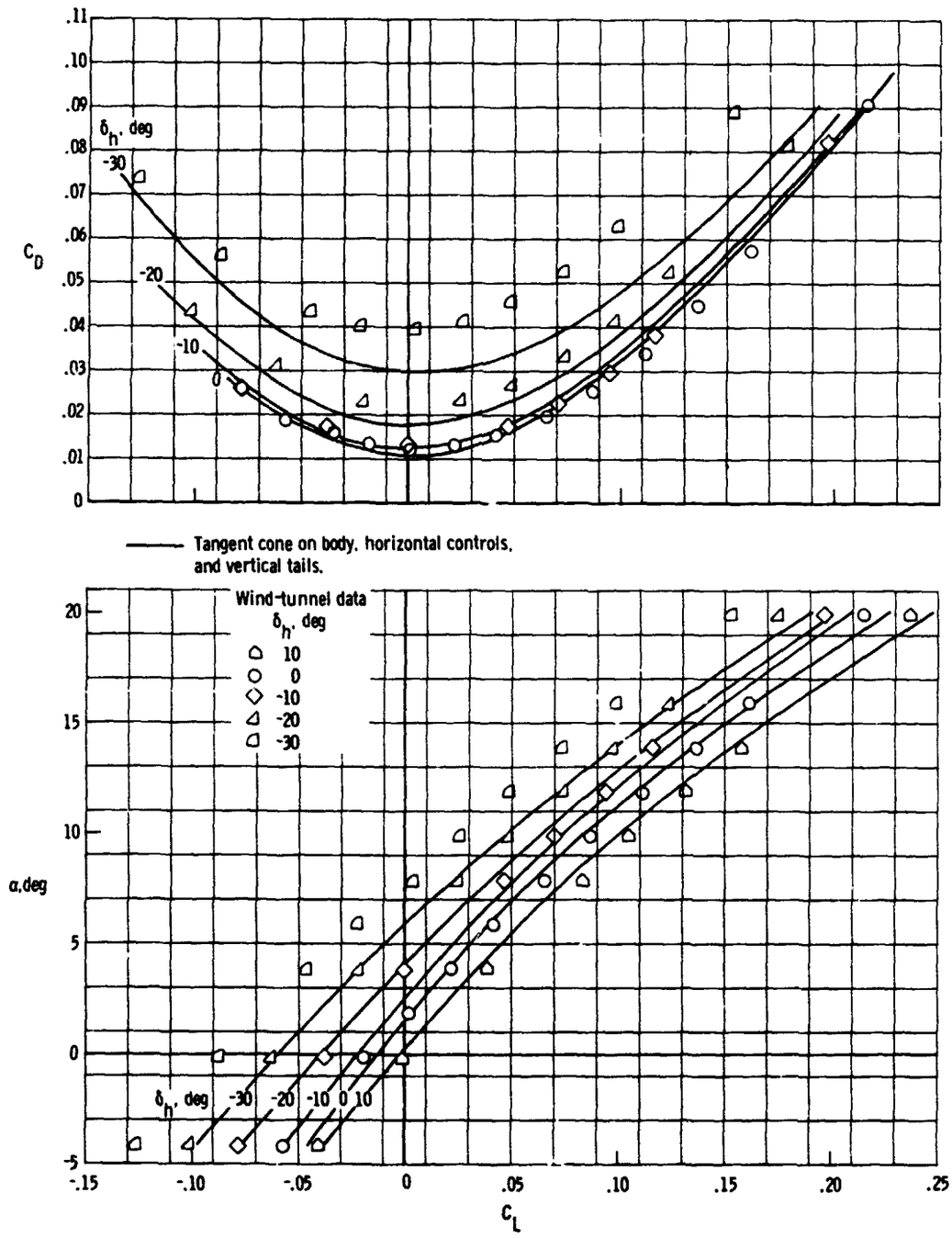

Figure 17.- Comparison of tangent-cone theory with wind-tunnel data for longitudinal aerodynamic characteristics of HYFAC configuration BHV at $R_{\infty,\ell} = 10.5 \times 10^6$.

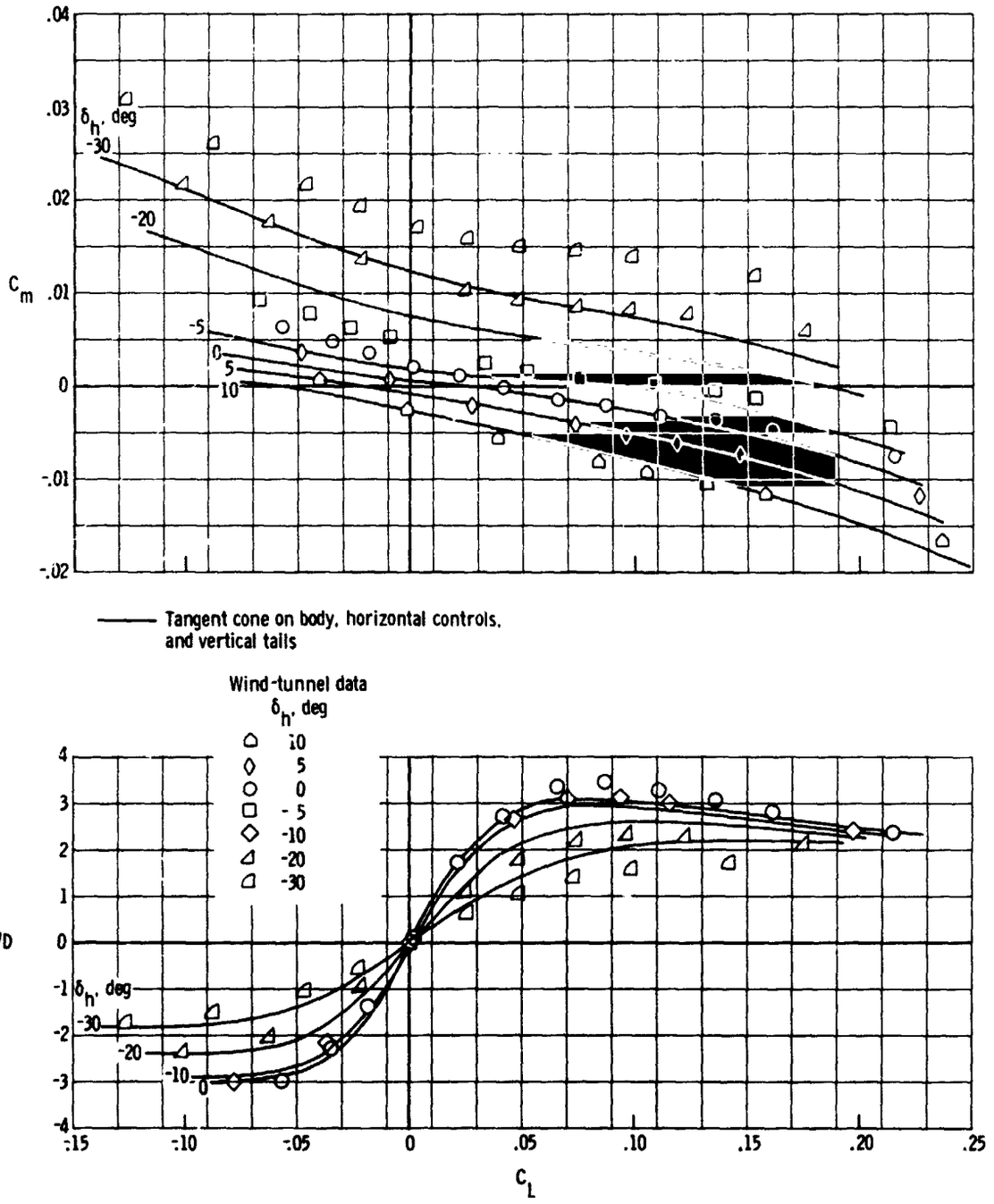

Figure 17.- Concluded.

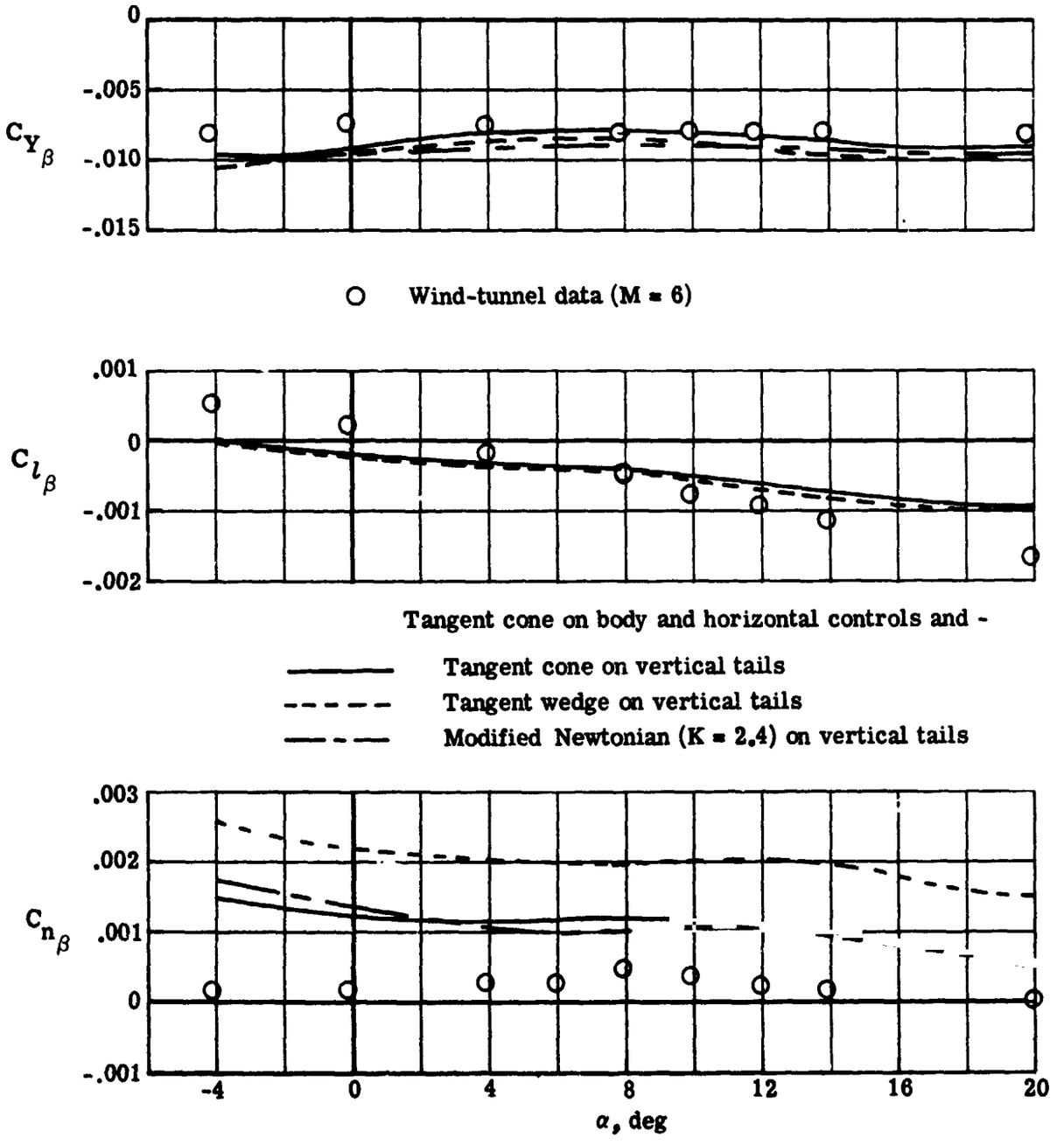

Figure 18.- Comparison of several hypersonic theories with wind-tunnel data for lateral-directional stability characteristics of HYFAC configuration (BHV). $\delta_h = 0^o$; $R_{\infty,\ell} = 10.5 \times 10^6$.

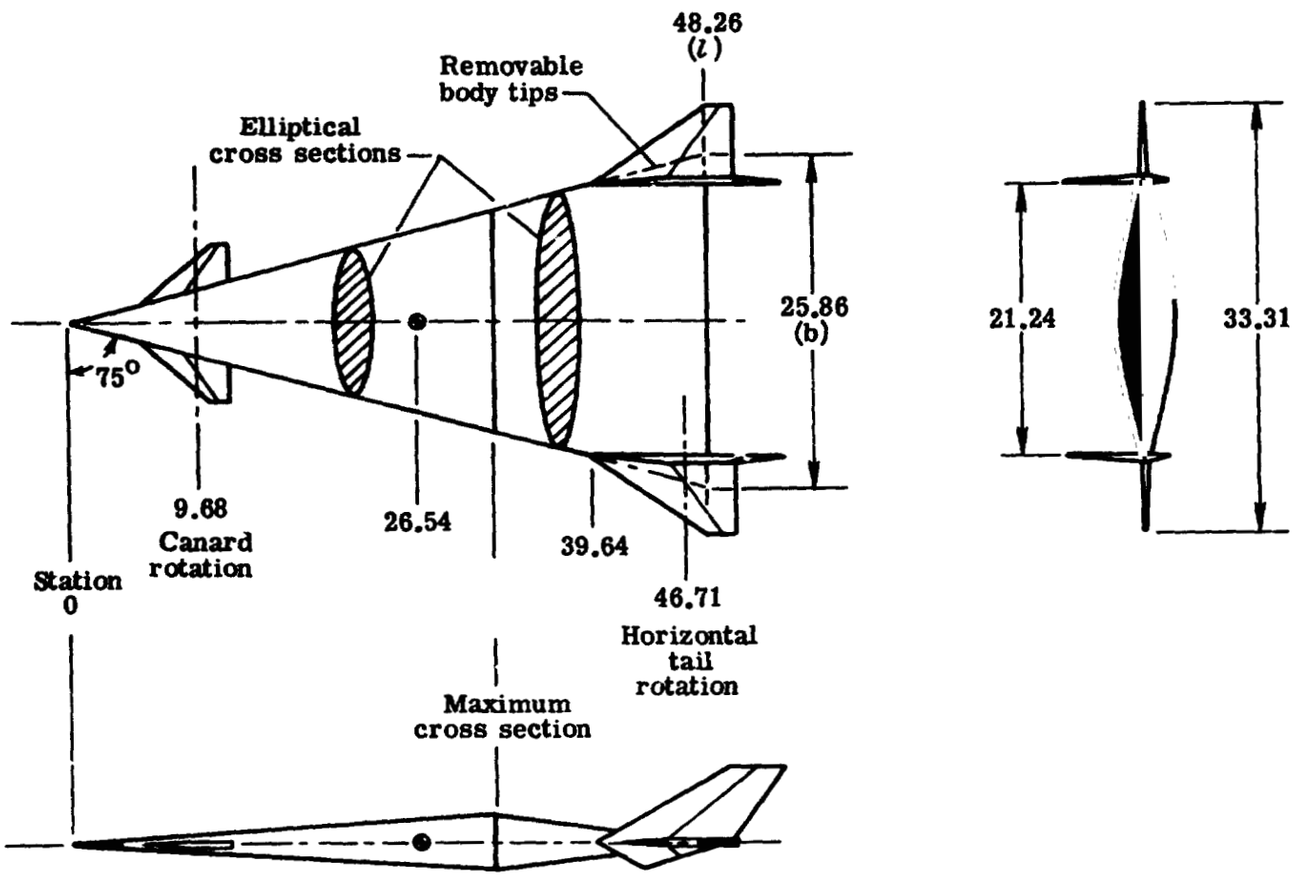

Figure 19.- Elliptical-cross-section configuration from reference 8. All dimensions are in centimeters.

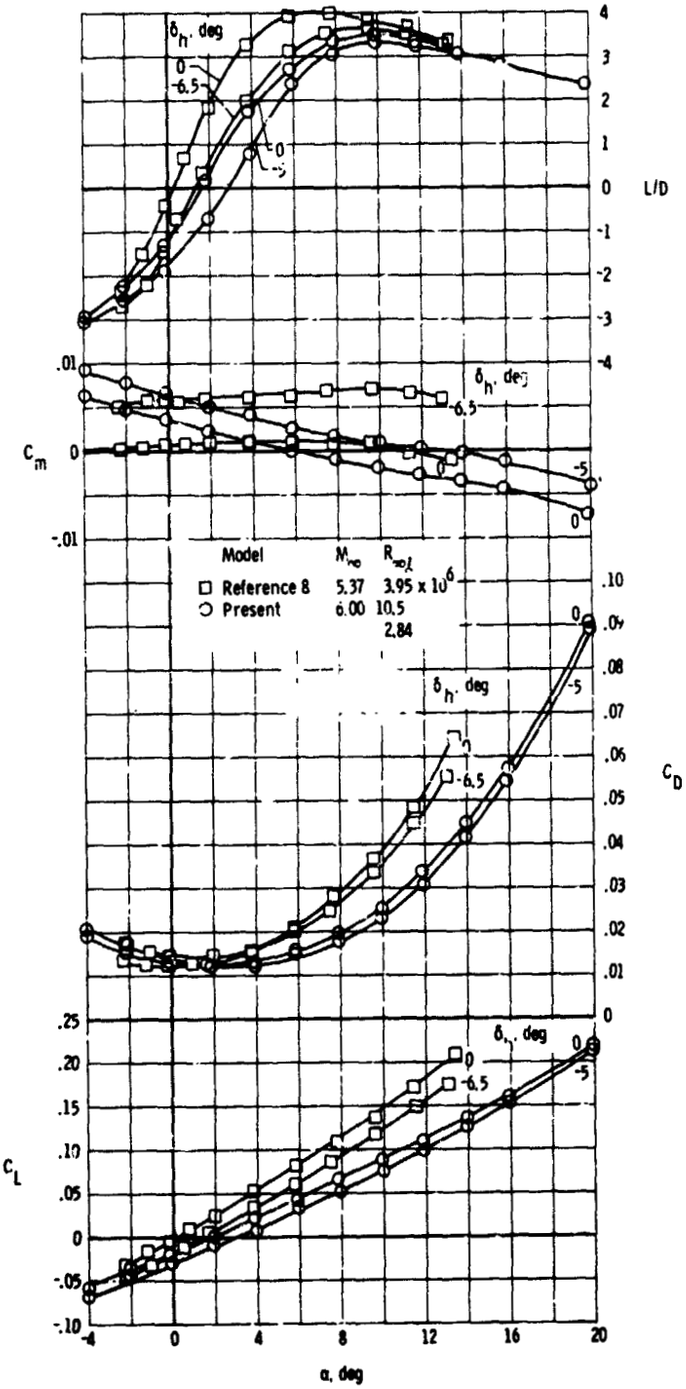

Figure 20.- Comparison of longitudinal aerodynamic characteristics of two all-body aircraft (BHV). Center of gravity at 0.64ℓ.

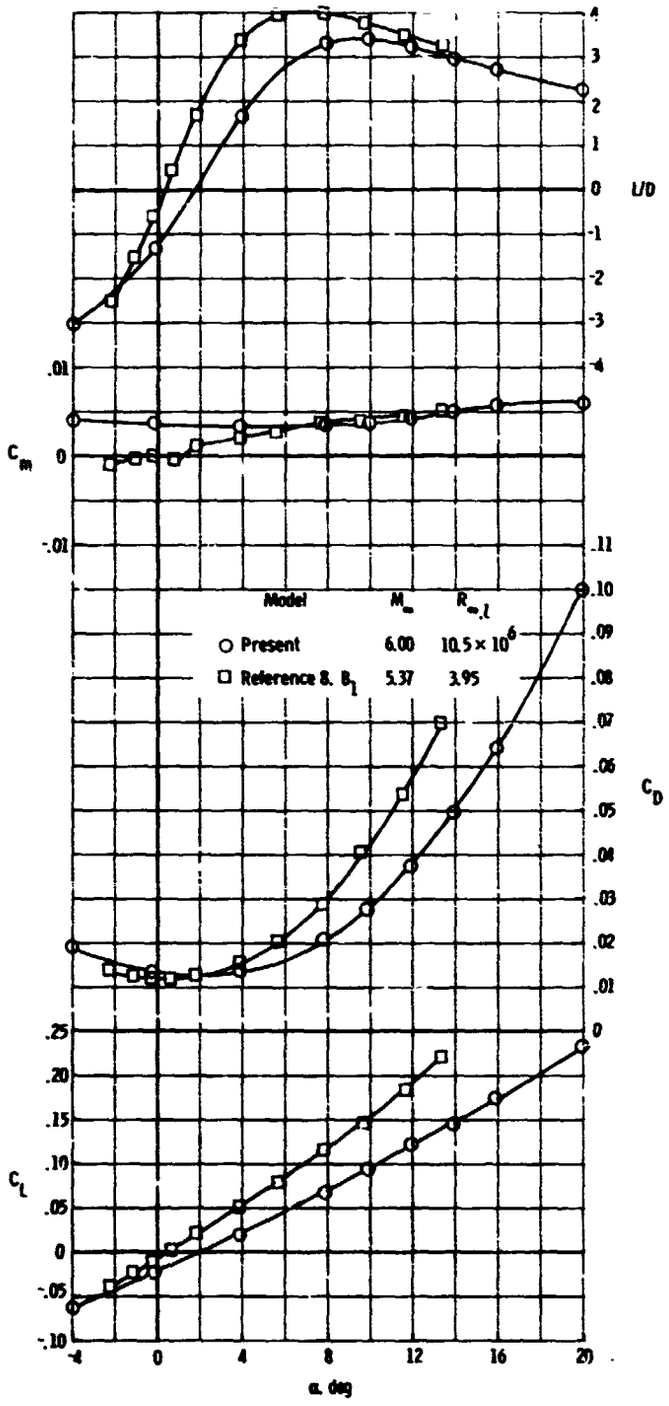

Figure 21.- Comparison of longitudinal aerodynamic characteristics of two all-body aircraft with canards ($BHVC_B$). $\delta_h = 0^o$; $\delta_c = 0^o$; center of gravity at 0.64l.

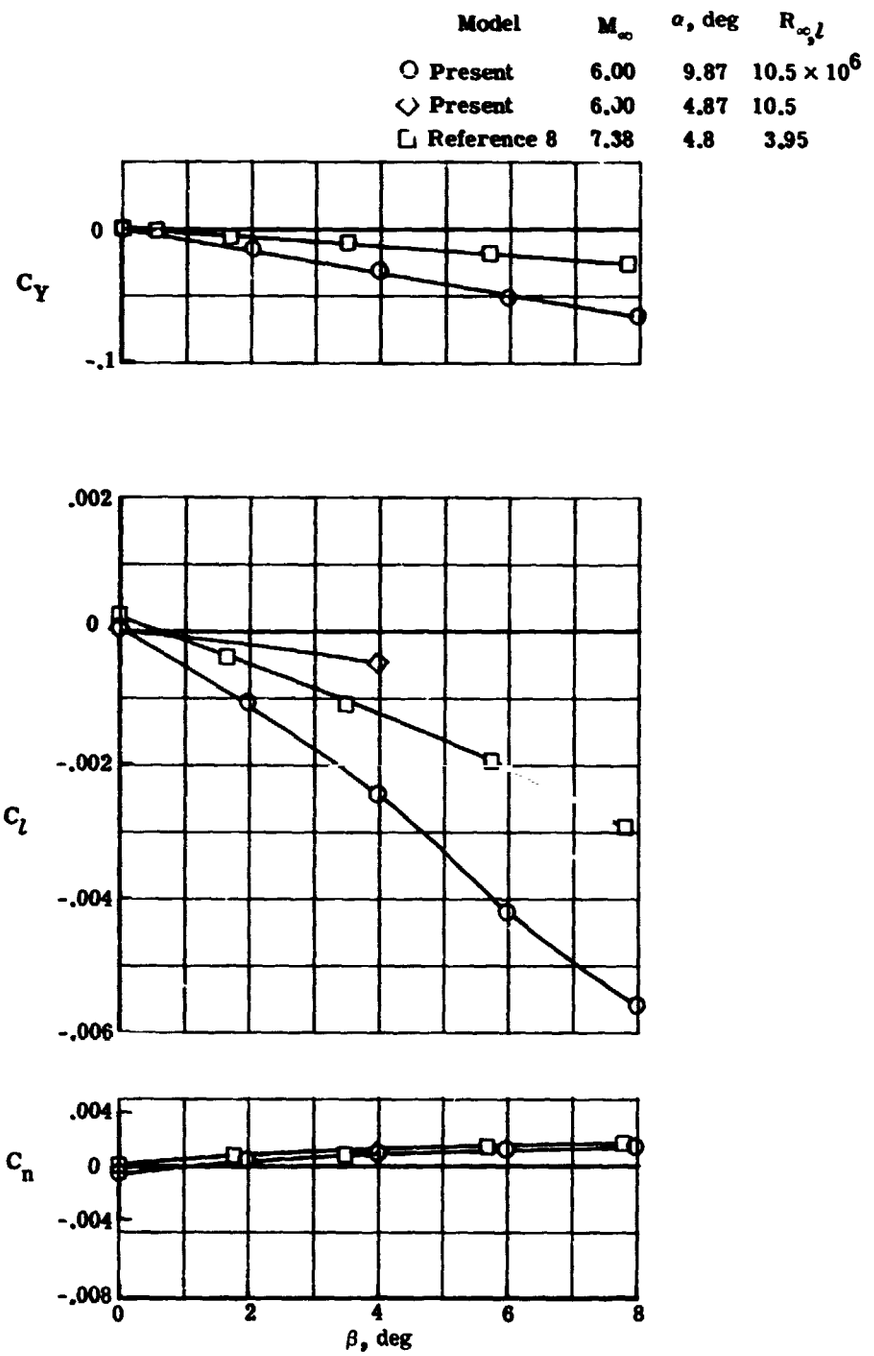

Figure 22.- Comparison of lateral-directional aerodynamic characteristics of two all-body aircraft (BHV). $\delta_h = 0^o$.

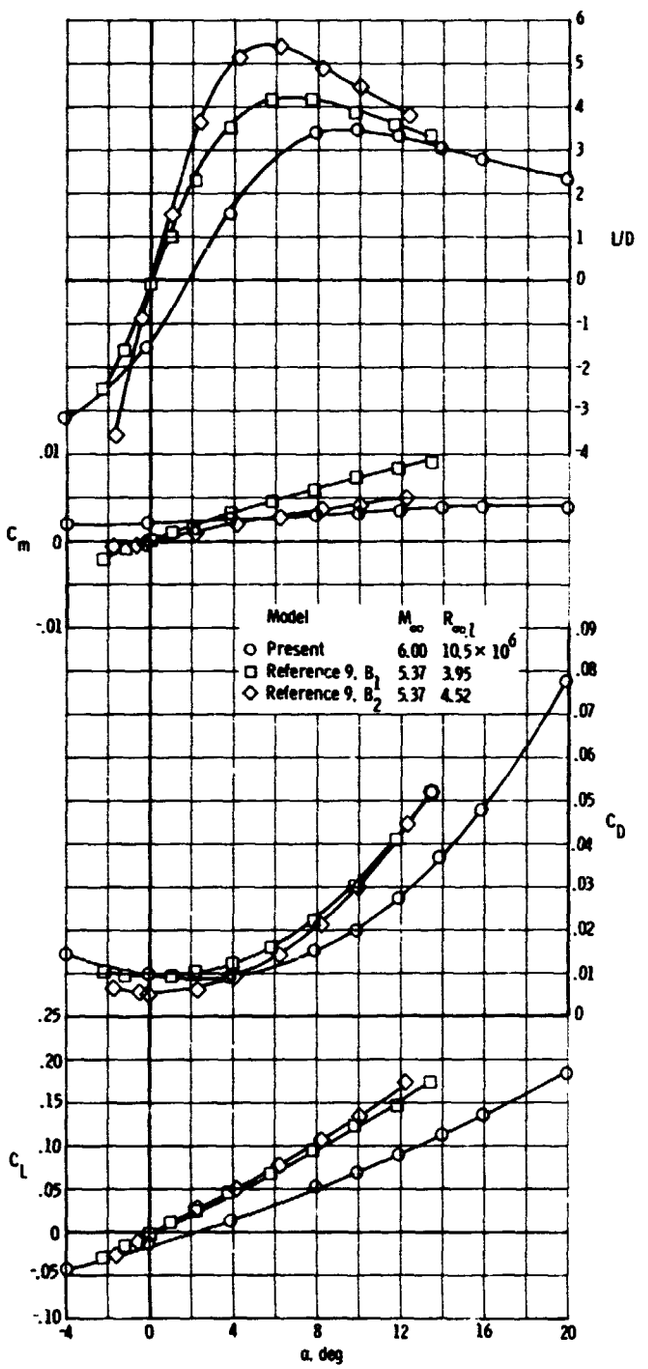

Figure 23.- Comparison of longitudinal aerodynamic characteristics of several lifting bodies (B). Center of gravity at 0.64l.

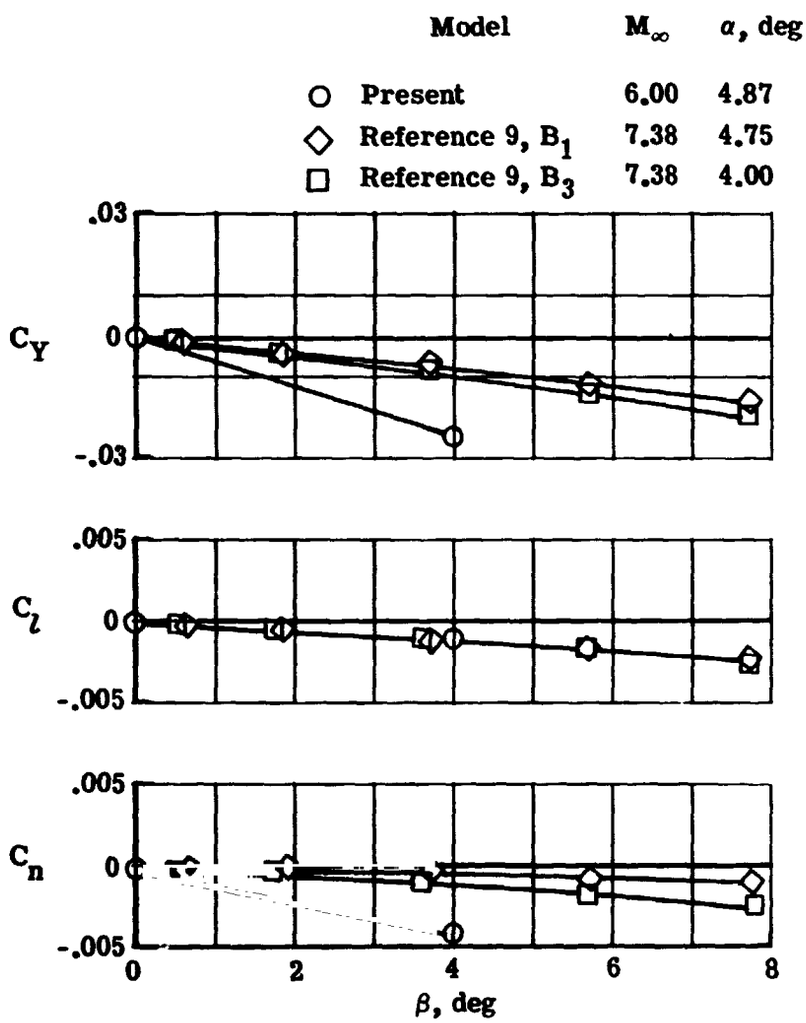

Figure 24.- Comparison of lateral-directional aerodynamic characteristics of several lifting bodies (B).

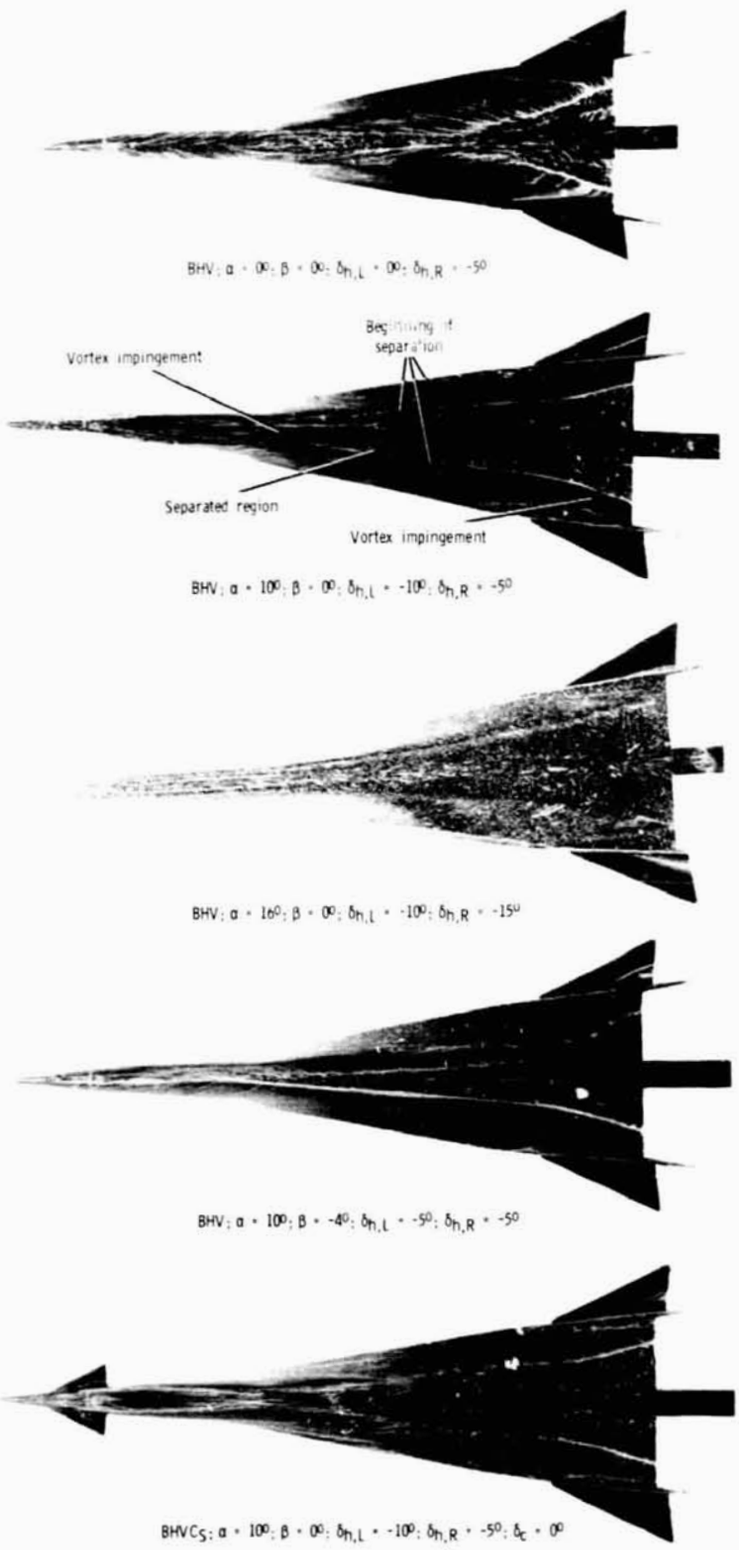

(a) Top view. L-73-6895

Figure 25.- Surface flow on HYFAC configuration. $M_\infty = 6$; $R_{\infty,\ell} = 10.5 \times 10^6$.

BHV: $\alpha = 0^{0}$; $\beta = 0^{0}$; $\delta_{h,L} = 0^{0}$; $\delta_{h,R} = -5^{0}$

BHV: $\alpha = 10^{0}$; $\beta = 0^{0}$; $\delta_{h,L} = -10^{0}$; $\delta_{h,R} = -5^{0}$

BHV: $\alpha = 16^{0}$; $\beta = 0^{0}$; $\delta_{h,L} = -10^{0}$; $\delta_{h,R} = -15^{0}$

BHV: $\alpha = 10^{0}$; $\beta = -4^{0}$; $\delta_{h,L} = -5^{0}$; $\delta_{h,R} = -5^{0}$

BHVC$_S$: $\alpha = 10^{0}$; $\beta = 0^{0}$; $\delta_{h,L} = -10^{0}$; $\delta_{h,R} = -5^{0}$; $\delta_c = 0^{0}$

(b) Side view. L-73-6896

Figure 25.- Continued.

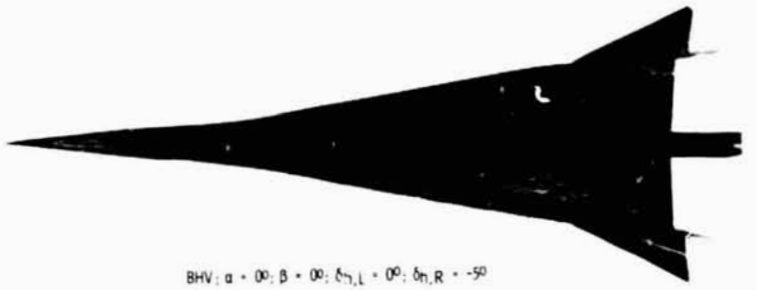

BHV; $\alpha = 0^0$; $\beta = 0^0$; $\delta_{h,L} = 0^0$; $\delta_{h,R} = -5^0$

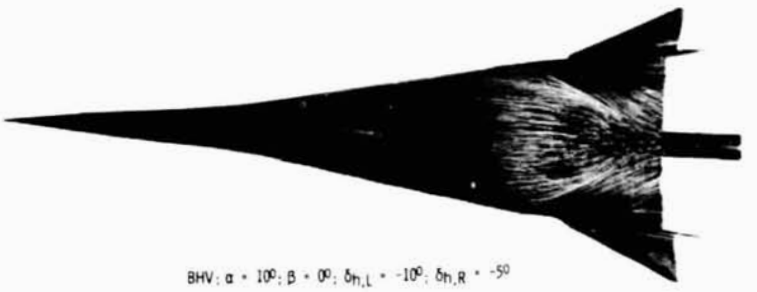

BHV; $\alpha = 10^0$; $\beta = 0^0$; $\delta_{h,L} = -10^0$; $\delta_{h,R} = -5^0$

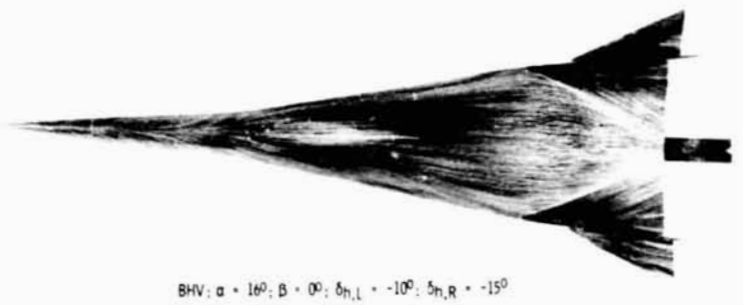

BHV; $\alpha = 16^0$; $\beta = 0^0$; $\delta_{h,L} = -10^0$; $\delta_{h,R} = -15^0$

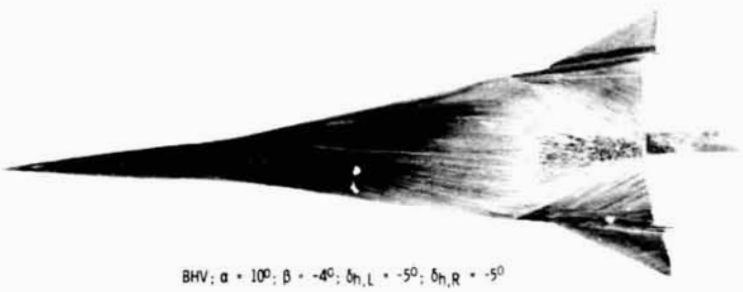

BHV; $\alpha = 10^0$; $\beta = -4^0$; $\delta_{h,L} = -5^0$; $\delta_{h,R} = -5^0$

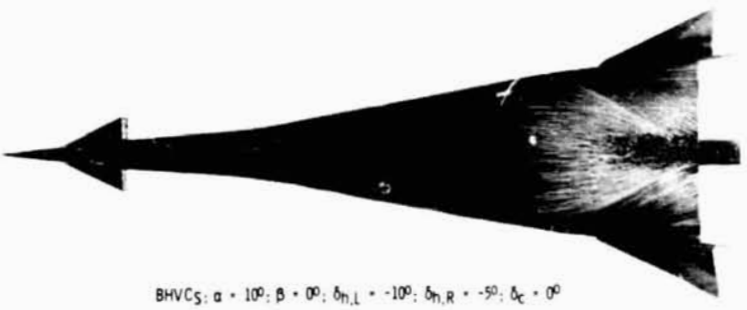

BHVCS; $\alpha = 10^0$; $\beta = 0^0$; $\delta_{h,L} = -10^0$; $\delta_{h,R} = -5^0$; $\delta_c = 0^0$

(c) Bottom view. L-73-6897

Figure 25.- Concluded.

NASA-Langley, 1973 — 2 L-8971